Characteristics and Environmental Conditions of Quasi-Stationary Convective Clusters during the Warm Season in Japan

Takashi Unuma* and Tetsuya Takemi

Disaster Prevention Research Institute, Kyoto University, Japan

*Correspondence to: Takashi Unuma, Gokasho, Uji, Kyoto 611-0011, Japan. E-mail: unuma_t@storm.dpri.kyoto-u.ac.jp

Quarterly Journal of the Royal Meteorological Society

Quarterly Journal of the Royal Meteorological Society

Page 2 of 66

Q. J. R. Meteorol. Soc. **00**: 2–39 (2013)

The characteristics and environmental properties of warm-season quasi-stationary convective clusters (QSCCs) in Japan were statistically investigated using operational weather radar and upper-air sounding data from May to October during 2005–2012. The characteristics of the environmental conditions for the development of QSCCs were described through a comparison with those for no-rain cases. We identified 4,133 QSCCs over the Japanese major islands. By compiling numerous QSCC samples, the horizontal scales of QSCCs on average and at the maximum with a circular shape are about 20 km and 72 km, respectively, indicating that warm-season QSCCs in Japan are meso-β-scale phenomena. The analyses of the environmental conditions for the QSCC and no-rain cases showed that the amount of moisture in the lower layer controls the stability condition for the development of the QSCCs, and that the magnitudes of the wind shear and the helicity in the lower troposphere distinguish the kinematic environments for the development of the QSCCs. An increase in the middle-level moisture leads to a larger amount of precipitable water vapor in the QSCC environments, suggesting that atmospheric moistening before the development stage of convection plays an important role in the development of the QSCCs. Additionally, the precipitation intensity has a higher correlation with the convective instability, whereas the precipitation area with the shear intensity. A comparison between slower- and the faster-moving CCs indicated that the precipitation intensity of the slower-moving CCs is stronger. This feature is related to a higher convective instability for the slower-moving ones.
Copyright © 2013 Royal Meteorological Society

1.   Introduction

Copyright © 2013 Royal Meteorological Society

Q. J. R. Meteorol. Soc. **00**: 2–39 (2013)

Understanding and predicting warm-season convective rainfall remain challenging tasks from both research and operational perspectives. Warm-season convective rainfall can sometimes be a significant event that spawns water-related disasters. Simply stated, heavier rainfall occurs where a high rainfall rate continues for an extended time (Chappell 1986; Doswell *et al.* 1996). As a cause of disaster-spawning heavy rain events, mesoscale convective systems (MCSs) act as key players among weather phenomena during the warm season. MCSs are defined as a cloud system that produces a contiguous precipitation area on the order of 100 km or more on a horizontal scale in at least one direction (Glickman 2000).

MCSs are widespread phenomena that develop in various climate regions ranging from tropical, sub-tropical, to extra-tropical regions. It is anticipated that locations with a stronger rainfall rate over an extended period will produce a heavier rainfall in the presence of a longer-lived MCS. From the Eulerian perspective, heavier rainfall is caused by the presence of a longer-lived and stationary (or slow-moving) MCS.

MCSs appear to be quasi-stationary due to two factors: 1) convective cells are continuously generated in similar locations by a back-building process (Bluestein and Jain 1985) under a stationary or slowly changing synoptic-weather condition (such as a stationary front), and 2) convective cells are continuously generated by topographic forcing. For example, Schumacher and Johnson (2008) examined an extreme rain event in the United States that occurred under quasi-stationary, synoptic-scale weather conditions where convective cells were successively generated by quasi-stationary forcings. On the other hand, complex topography plays a role in triggering and enhancing flash-flood-producing events over the Alpine region (e.g., Buzzi and Foschini 2000; Anquetin *et al.* 2003; Davolio *et al.* 2009; Panziera *et al.* 2014). In addition,

quasi-stationary convective systems found in the southern part of the United Kingdom develop due to forcing from sea breezes (Warren *et al.* 2014).

[Figure 1 about here.]

Quasi-stationary convective systems are a well-known cause of heavy rainfall in Japan. Such events frequently appear during the warm season (Ogura 1991; Yoshizaki and Kato 2007) under the presence of extra-tropical cyclones, synoptic-scale fronts, tropical cyclones, or stationary fronts such as Baiu fronts. The horizontal scale of a precipitating system over Japan is typically on the order of 10 km, which corresponds to the meso-β-scale by the definition of Orlanski (1975).

The environmental conditions necessary to develop quasi-stationary convective systems, particularly during the Baiu season, are characterized by a larger moisture content (Kato 2006; Hirockawa and Kato 2012). Higher environmental moisture may be a common feature for MCS events over East Asia; for example, Meng *et al.* (2013) showed that precipitable water is higher for the MCSs in east China than for those in the United States. In addition to such humid conditions, kinematic effects such as low-level convergences and vertical shears of horizontal winds play important roles in maintaining quasi-stationary convective systems (Kato 1998; Kato and Goda 2001; Kato and Aranami 2005; Yoshizaki *et al.* 2000). Kato (2005) examined the conditions favorable for the development of quasi-stationary convective systems over Kyushu Island, which is located in the western part of Japan, and found that the presence of persistent southwesterly winds is required to form quasi-stationary convective systems. In addition, Yoshizaki *et al.* (2000) showed that topographic forcing is important to

56 trigger convective clouds and organize quasi-stationary convective systems over the western

57 part of Kyushu Island. In this way, many studies have investigated quasi-stationary convective

58 systems with significant societal impacts and/or have employed special campaigns as a case-

59 study basis.

60   However, few have investigated the statistical or climatological features of quasi-stationary

61 convective systems in Japan by compiling numerous samples. One exception was conducted

62 by Chuda and Niino (2005); through an investigation of the features of the background

63 atmospheric conditions over Japan in terms of environmental parameters using radiosonde

64 data, they showed that the environmental parameters strongly depend on the location and

65 the season. Convective available potential energy (CAPE) values generally become larger at

66 lower latitudes and during the warmer season; thus, convective storms favor to develop in the

67 southern parts of Japan during the warmer season. Because their study did not distinguish the

68 environmental conditions for convective events from non-convective events, the environmental

69 characteristics for the development of quasi-stationary convective systems in Japan remain

70 unknown.

71   The distinction between convective and non-convective environments should help our

72 understanding on the general conditions necessary to develop convective precipitation. A

73 statistical analysis for afternoon thunderstorms over the Kanto area (see Figure 1(b)) in the

74 summer was conducted by (Nomura and Takemi 2011). Nomura and Takemi examined 11

75 environmental parameters for afternoon rain cases by comparing with no-rain cases with the

76 use of mesoscale-gridded analysis data by Japan Meteorological Agency (JMA) as well as the

77 radiosonde data observed at Tateno (see Figure 1(b)). The K Index significantly distinguishes

the environmental conditions between the rain and the no-rain cases. They also investigated the vertical structures of temperature and moisture, and concluded that colder temperatures at middle levels and higher humidity at low to middle levels are the conditions favorable for afternoon rains.

A similar analysis was conducted for afternoon rain events in and around the Nobi Plain located in central Japan (Takemi 2014a). In addition, Kato (2006)'s case studies suggested that the middle-level moisture plays an important role in determining the development of convective systems. However, statistical studies that specifically focus on quasi-stationary convective systems have yet to be conducted. In this study, which focuses on various types of convective systems, including a cluster of convective clouds, we refer to quasi-stationary convective systems as quasi-stationary convective clusters (QSCCs).

The purpose of this study is to reveal the climatological features of QSCCs, including lifetime, location, rain intensity, and the environmental properties for the development of QSCCs during the warm season over Japan. The analyses were performed using operational radar and upper-air observation data. To identify QSCCs, we modified a method to detect an individual convection cell within a precipitating area from radar observations (Shimizu and Uyeda 2012). The environmental characteristics for the development of QSCCs were examined in terms of the environmental parameters by comparing QSCC events and no-rain cases using idea similar to Nomura and Takemi (2011) and Takemi (2014a). From the environmental analyses, we revealed the conditions favorable for the development of QSCCs from a climatological point of view. Because Barnes and Sieckman (1984) showed that there are similarities and differences of the environments for fast- and slow-moving

mesoscale convective cloud lines over the tropics, we also examined the differences of the

characteristics and environmental properties of QSCCs by dividing them into sub-groups

based on their propagation speed (i.e., slower-moving CCs and faster-moving CCs). Through

a demonstration of the specific parameters used to diagnose the development of QSCCs, it is

emphasized here that statistical information can be used as a better forecasting guide for the

development of QSCCs.

2.   Data and methodology

2.1.   Data

The data observed during the warm season, i.e., from May to Octorber, during 2005–2012

are used in this study. To identify QSCCs, we use operational radar data of JMA. In this

dataset, the radar reflectivities from 19 elevation angles within the detection range of 200 km

are converted to precipitation intensities at the height of about 2 km. This study uses this

precipitation intensity dataset. The unit of the data is mm h^{-1}. The horizontal resolutions

on the longitude-latitude grid is approximately 1 km (hereafter referred to as 1 km), and

the temporal interval is 10 minutes, which are sufficiently high for identifying and tracking

QSCCs all over Japan. Since the present study deals with QSCCs that develop over land, the

area for the analysis of the radar precipitation intensity is limited to the Japanese major islands

and the surrounding region within 10 km off the coast. The locations and ranges of those radars

are shown in Figure 1(a).

The upper-air sounding data by radiosondes are used to examine the environmental

conditions for the development of the extracted QSCCs. Figure 1(b) shows the locations

121 of these stations: Wakkanai (WKN), Sapporo (SPR), Kushiro (KSR), Nemuro (NMR),

122 Akita (AKT), Wajima (WJM), Tateno (TTN), Hamamatsu (HMT), Matsue (MTE), Yonago

123 (YNG), Shionomisaki (SNM), Fukuoka (FKO), and Kagoshima (KGS). Note that the Nemuro

124 (Yonago) station was re-located to Kushiro (Matsue) in March 2010, and thus the Nemuro

125 (Yonago) station is regarded as the same with the Kushiro (Matsue) station. We consider that

126 the differences that may arise owing to this re-location are minimal in the analysis on the

127 environmental conditions because the re-located stations belong to similar climate regions.

128 The times of the upper-air observations are 0900 and 2100 Japan Standard Time (JST), which

129 is 9 hours plus UTC. Hereafter the times are referred to as JST.

2.2. *Identification and tracking of QSCCs*

131 To extract QSCCs, we use Algorithm for the Identification and Tracking Convective Cells

132 (AITCC) that was developed by Shimizu and Uyeda (2012). This algorithm was originally

133 intended to identify and track individual convective cells within an MCS. We modify the

134 algorithm for identifying and tracking QSCCs. The procedures of how to extract QSCCs are

135 described here.

136 The first procedure is to extract convective clusters (CCs). At every time step, we define

137 a contiguous area of the precipitation intensity that is equal to or greater than a prescribed

138 threshold from the radar observations (Figure 2(a)). The minimum threshold is set to be 10

139 mm h^{-1}, corresponding to about 40 dBZ from the reflectivity-rainfall intensity relationship

140 used by JMA, in order to extract convective regions. The threshold of 40 dBZ, which was used

141 by Steiner *et al.* (1995) and Geerts (1998) to identify convective echoes, is modified from the

142 original AITCC algorithm that uses the threshold of 30 dBZ (Shimizu and Uyeda 2012). If the

143 contiguous area is equal to or greater than 200 km^2, the precipitation area is defined as a CC

144 (Figure 2(b)). In most cases, multiple CCs are extracted at every time step. These extracted

145 CCs are labeled with different identification numbers (ID) as shown in Figure 2(b).

146   The second procedure is to identify quasi-stationarity of CCs. Here we track the extracted

147 CCs in time series and identify the lifetime of the QSCCs (Figure 2(c) and 2(d)). Figure 2(c)

148 schematically depicts the centroids and defined areas of two CCs: one at time t = T; and the

149 other at t = T + dt (dt: the time difference). From these CCs, an overlapped-area is determined

150 by the areas of the CCs at t = T and t = T + dt (Figure 2(d)). At the same time, a motion

151 vector is defined by pointing the centroid of the CC at t = T + dt from that of the CC at t = T

152 (Figure 2(c)). Figure 2(d) displays the case where a part of the CC at t = T and a part of the

153 CC at t = T + dt are overlapped. The magnitude of motion vector and the size of an overlapped

154 area are used to determine the identity of a CC. The threshold of the maximum motion vector

155 and the minimum overlapped area were set to be 16.7 m s^{-1} and 1 km^2 (corresponds to 1

156 grid point in the 1-km horizontal resolution of the radar data), respectively, in the original

157 algorithm of Shimizu and Uyeda (2012). The threshold for the motion vector is changed to 10

158 m s^{-1} in the present study. Thus, if the magnitude of the motion vector is equal to or smaller

159 than 10 m s^{-1}, the CC at t = T + dt is regarded as the same system with the CC at t = T. In this

160 way, QSCCs are defined.

161   When a CC at t = T has multiple candidates at t = T + dt in this tracking procedure, a single

162 CC that is the most likely linked to the CC at t = T is determined with the tracking algorithm

163 of AITCC (see details in section 2.4 of Shimizu and Uyeda 2012). When a CC at t = T has

Copyright © 2013 Royal Meteorological Society

Q. J. R. Meteorol. Soc. **00**: 2–39 (2013)

164 no candidate CCs at t = T + dt, the tracking algorithm stops. This time t = T is defined as the

165 end of the lifetime of a QSCC. Here, the QSCCs whose lifetime is less than 20 minutes are

166 excluded, because the lifetime should be resolved by at least three time steps of the radar data.

167 A possible limitation of the present method is that the method is not able to track a CC which

168 propagates discretely; if there are no overlapping areas of CCs at t = T and t = T + dt, the CCs

169 are not classified as the same CC. This limitation may bias the results toward shorter lifetimes.

170 [Figure 2 about here.]

171 *2.3. Environmental indices and parameters*

172 Environmental conditions before the development of the extracted QSCCs are investigated

173 with the use of upper-air sounding data. For each QSCC, a sounding station which is within

174 the 200 km range from and the nearest to the centroid of the QSCC is used. The atmospheric

175 conditions at times within 1–9 hours prior to the developments of the extracted QSCCs are

176 defined as the environments before the QSCC occurrence; the sounding data at these times are

177 used for the present analysis. In other words, we do not use data at 0–1 hour and 10–11 hour

178 before the QSCC development, because the data at 0–1 hour before may strongly be affected

179 by QSCCs themselves and the data at 10–11 hour before may not reflect the environments

180 before the development of QSCCs.

181 The environmental conditions are diagnosed in terms of indices and parameters related

182 to static stability and vertical wind shear. There are a number of environmental indices and

183 parameters that are related to stability and shear conditions (e.g., Markowski and Richardson

184 2010). The parameters examined here are convective available potential energy (CAPE),

convective inhibition (CIN), precipitable water (PW), Showalter Stability Index (SSI), K Index

(KI) (George 1960), temperature lapse rate from 850 to 500 hPa (TLR) (Takemi 2007a,b),

0–3 km mean shear (MS03) (Rasmussen and Blanchard 1998), and 0–3 km environmental

helicity (EH03) (Davies-Jones 1984). CAPE is calculated by adiabatically raising a parcel

whose properties are vertically averaged in the lowest 500 m; in calculating CAPE the effects

of condensate loading, entrainment, and latent heat of fusion are neglected, and buoyancy is

defined with virtual temperature. In cases when the level of free convection is not identified,

the values of CAPE and CIN are not obtained and hence not used for the statistical analyses

described later. Choosing the 850-hPa and 500-hPa levels for the TLR calculation is based

on an idea of comparing the effects of lapse rate and moisture in the definition of KI. The

environmental property of EH03 is used to see how large the hodograph curvature is.

Another important factor for the development of QSCCs is a lifting effect. However, we do

not address the lift due to the limitation of the radiosonde observations, which indicates the

difficulty in estimating large-scale lifting from a single sounding.

For the purpose of comparing the environmental conditions before the development of the

extracted QSCCs, environmental conditions for no-rain cases are also examined. The no-rain

cases are defined as having no radar-observed precipitation at any grid points within the 200-

km distance from the radiosonde sites between the observation times. It should be noted that

once a radiosonde observation is associated with a certain QSCC, it is no longer used for other

QSCCs or a no-rain case. A single observation is only used once and counted only once for the

Copyright © 2013 Royal Meteorological Society

Q. J. R. Meteorol. Soc. **00**: 2–39 (2013)

composite. Statistical significance of the differences of the environmental parameters between the QSCCs and the no-rain cases is also examined[1].

3. Results

3.1. General characteristics of the extracted QSCCs

In this subsection, we will present overall characteristics of the extracted QSCCs. The total number of the extracted QSCCs are 4,133, while the total number of no-rain cases for a comparison purpose is 99,673[2].

The frequency distribution of the temporal and spatial means of precipitation intensity averaged for all the QSCCs is shown in Figure 3. Note that by definition the minimum value of the mean precipitation intensity is 10 mm h^{-1} (see section 2.2). A peak in the frequency distribution is seen at 20 mm h^{-1}, while the mean, median, and maximum values are 22.3, 21.5 and 54.0 mm h^{-1}, respectively. The frequency of the averages of precipitation intensity that is equal to or smaller than 30 mm h^{-1} is 93%.

[Figure 3 about here.]

Figure 4 shows the frequency distribution of the temporal mean of precipitating area for all the QSCCs averaged during their lifetimes. By definition the minimum value is 200 km^2. The frequency decreases with the increase in the precipitation area. Because of the shape of the distribution, the mean and median values are different with each other: 329 and 286

---

[1] Student's t-test is used to show the statistical significance in this study. If a distribution shows the one tail, Mann–Whitney U test will be additionally applied.

[2] This number means the number of the detected events on the radar data. Note that the actual total number for the no-rain environments is reduced to 7,619 (see details Figure 8 and the related descriptions).

223 km^2, respectively. The number of events with a large precipitation area becomes significantly

224 reduced; the upper limit of the mean precipitation area identified in this analysis is 3,961

225 km^2. If these areas are assumed to have a circular shape, the mean and the maximum radius

226 equivalent to a circle is about 10 km and 36 km, respectively. Thus, it can be assumed that

227 typical sizes of the QSCCs with a circular shape assumed are about 20 km on average and

228 72 km at the maximum. The examination of the sizes of the extracted QSCC at all the time

229 steps indicated that the maximum QSCC area is 10,616 km^2, which is one fifth of a mesoscale

230 convective complex (e.g., Maddox 1980) of 50,000 km^2 with the threshold of temperature that

231 is less than or equal to -52 degree C as a typical cloud area. This maximum area corresponds

232 to the equivalent radius of 58 km, which indicates that the maximum horizontal size of QSCCs

233 is about 120 km. Therefore, it is simply stated that the QSCCs in Japan are meso-β-scale

234 phenomena. The horizontal scale of the QSCCs at their mean is smaller than that of a typical

235 MCS, i.e., meso-α-scale (Glickman 2000). This is considered to be related to their shear

236 environments, which will be examined in sections 3.4 and 3.5.

237   [Figure 4 about here.]

238   Examining the lifetimes of QSCCs indicates that the frequency of QSCCs lognormally

239 decreases with the increase in the lifetime (Figure 5). Ninety five percent of the extracted

240 QSCCs have a lifetime of less than 60 minutes. There is a slight change in the slope of the

241 distribution at around the lifetime of 60 minutes. This means that a number of QSCCs with a

242 longer lifetime becomes rapidly reduced.

243   [Figure 5 about here.]

244   The spatial distribution of the occurrence of QSCCs is shown in Figure 6(a). The location of

245   each QSCC is defined as a point at which the QSCC is initially identified during the tracking

246   procedure. A number of events is assessed in a unit area of 50 km by 50 km in order to

247   see general characteristics by filtering out small-scale features. It is seen that QSCCs occur

248   frequently on the Pacific side of the Japanese islands and the western part of Japan. Frequent

249   occurrence is also seen on the Japan Sea side and the inland regions in central Japan. The

250   frequency is generally lower in northern Japan than in the other regions. By comparing the

251   spatial pattern in Figure 6(a) with terrain feature (Figure 1(a)), we can also note that overall

252   the points with the frequency of greater than or equal to 30 correspond well to regions with

253   high elevation and/or near mountainous topography.

254   To see how the amount of rainfall induced by QSCCs contributes to the total amount of

255   rainfall during the warm season, the percentage of the total rainfall due to the extracted

256   QSCCs to the total amount of rainfall during the warm season is examined and is shown in

257   Figure 6(b). The percentage is seen to be higher in the western part and the Pacific side of the

258   Japanese islands. In particular, higher values of greater than 3% are found over Kyushu, the

259   southwestern part of Shikoku, the southern part of Kinki, and the north and the northwestern

260   part of Kanto. The spatial distribution of the occurrence of the QSCCs may be associated with

261   a regional feature of the environmental parameters, which will be mentioned in section 3.3.

262   Based on Figure 6, the whole analysis region of Japan is divided into three regions. The

263   first region is the Hokkaido region, where both the frequency and the rainfall contribution

264   of QSCCs are the lowest. Regions with higher frequency are divided into the Japan Sea side

265   region, and the Pacific side region. The radiosonde sites in the Hokkaido region are WKN,

266 SPR, KSR, and NMR; those in the Japan Sea side region are AKT, WJM, YNG, and MTE;

267 and those in the Pacific side region are TTN, HMT, SNM, FKO, and KGS. As a representation

268 of each region, the stations of SPR, AKT, and KGS are chosen for the Hokkaido, the Japan

269 Sea side, and the Pacific side region, respectively (e.g., Chuda and Niino 2005). By dividing

270 the whole analysis area in this way, the environmental conditions for the QSCC development

271 are examined, which will be described in section 3.2.

272   [Figure 6 about here.]

273 The temporal change of the QSCC characteristics during the warm season is investigated as

274 a monthly basis. Figure 7 exhibits the monthly changes in the total numbers of the QSCCs.

275 The number of the QSCCs exceeds 500 from July to September, having a peak in August,

276 while that in May and October becomes largely reduced. The higher frequency of the QSCCs

277 is considered to be due to Asian monsoon activity (rainy season) in June and July, and eventual

278 tropical cyclones and stationary fronts from August to September. One thing to be noted here

279 is that, the rainbands associated with tropical cyclones are included in the extracted QSCCs in

280 this study, because we investigate various types of convection.

281   [Figure 7 about here.]

282 To show how frequent rainfall events occur during the warm season, we examine the

283 percentage of the number of no-rain cases to the total number of the radiosonde observation

284 times. Figure 8 shows the month-to-month change of this no-rain percentage as well as the

285 actual number of no-rain cases. In contrast to the features found in Figure 7, it is seen from

286 Figure 8 that the percentage and the actual number of the no-rain cases are lower from July to

Copyright © 2013 Royal Meteorological Society

Q. J. R. Meteorol. Soc. **00**: 2–39 (2013)

287 September, while that is the highest in May. Although the features of June and October seem

288 to be similar, the occurrence of QSCCs is lower in October than in June (Figure 7).

[Figure 8 about here.]

290 Based on the monthly features shown in Figures 7 and 8, the warm season from May to

291 October is categorized into three sub-seasons. May and October are in spring and autumn,

292 respectively, and are summarized as the same sub-season, referred to as Season 1 (denoted as

293 S1). June, which belongs to a rainy season because of the higher activity of Asian monsoon, is

294 defined as Season 2 (hereafter S2). July-August-September is defined as Season 3 (hereafter

295 S3). Based on this categorization, the environmental properties of QSCCs are investigated in

296 the following section.

3.2. *Vertical structure of the environmental atmosphere*

298 In this subsection, we examine the vertical structure of the environmental atmosphere for

299 the development of the extracted QSCCs (denoted as Q category) by comparing with those for

300 the no-rain cases (denoted as N category). Hereafter, the Q and N categories are referred to as

301 Q and N. The vertical profiles of SPR, AKT, and KGS are averaged in each season, i.e., S1,

302 S2, and S3.

303 Firstly, the characteristics of the vertical profiles of temperature, moisture, and wind are

304 described to provide overall views for the stability and shear conditions that will be given in

305 the next subsection. The vertical profiles of temperature, water vapor mixing ratio, and relative

306 humidity for Q and N are shown in Figure 9. A common feature found in the temperature

307 profiles is that temperatures under the level of 850 hPa and above the level of 400 hPa are

308 higher in Q than in N for all the three sites in all the seasons (Figures 9(a), 9(d), 9(g)), which

309 are statistically significant at a confidence level of 95% (Figures 10(a), 10(d), 10(g)). On the

310 other hand, temperatures at the middle levels do not show a consistent feature between Q and

311 N, although they are a little higher in Q than in N. Note that the T-values at the 600- and 700-

312 hPa levels are smaller, which suggests that the statistical significance of the difference may be

313 marginal. The smaller T-values at the middle levels are also seen in HMT, MTE, and YNG in

314 the season of S3 (see Figures SI-6(d) and SI-7(d) of Supporting Information).

315 In contrast to the temperature profiles, the difference of water vapor mixing ratio and relative

316 humidity between the categories is clearly identified. Water vapor mixing ratio and relative

317 humidity throughout the troposphere are higher in Q than in N for all the three sites in all

318 the seasons (Figures 9(b), 9(c), 9(e), 9(f), 9(h), 9(i)). The differences described above are

319 also statistically significant at a confidence level of 95% (Figure 10(b), 10(c), 10(e), 10(f),

320 10(h), 10(i)). On the other hand, there are no significant differences of the water vapor mixing

321 ratio between Q and N at the lower and upper troposphere in S2 of SPR (Figure 10(b)). This

322 feature is also seen in WKN in the seasons of S1 and S2 (see Figures SI-1(b)–(c) and SI-

323 5(b)–(c) of Supporting Information). Considering these features, it should be noted that the

324 environments for the development of QSCCs are characterized as both higher temperature at

325 the lower troposphere and larger moisture throughout the troposphere during the warm season

326 in Japan. These differences of temperature and moisture between the categories will affect the

327 diagnosis of stability conditions, which will be described in the next subsection.

328   [Figure 9 about here.]

329 [Figure 10 about here.]

330 The features of the wind profiles can be obtained from the hodographs. Figure 11 compares

331 the mean wind hodographs in Q and N depending on the site and the season. The differences in

332 the shapes of the hodograph between the categories are clearly seen. The shapes in Q indicate

333 a clockwise veering feature from the surface to about 700 hPa and a nearly unidirectional

334 structure above that level. On the other hand, in N, a wind veering is not seen at the lower

335 levels, while slight anti-clockwise feature can be identified at the middle-to-upper levels in

336 some sites/seasons. One of the pronounced features on the hodograph curvatures in Q is that

337 easterly winds are seen at the lower troposphere at all the three sites (Figures 11(a)–(c)). This

338 feature is mostly seen over the Pacific side in the season of S1, which is related to larger

339 hodograph curvature in Q. In addition, the hodograph shapes and the direction of rotation

340 strongly depend on the meridional wind at all the three sites in all the seasons. Most of these

341 differences of zonal and meridional winds between Q and N are statistically significant at a

342 confidence level of 95% (Figure 12), except for the zonal wind in the seasons of S1 and S2

343 (Figures 12(a), 12(c), 12(e)). The significant difference seen here corresponds to the difference

344 of the hodograph curvature between Q and N. The statistical difference suggests that the

345 clockwise veering in Q and the anti-clockwise veering in N control the shear condition for

346 the development of QSCCs.

347 [Figure 11 about here.]

348 [Figure 12 about here.]

349   If the environmental winds are assumed to be geostrophic winds, there is warm advection

350 associated with the clockwise veering feature in Q (in terms of thermal wind balance). In

351 addition, the hodographs in Q are consistent with the environments on the warmer side of

352 warm or stationary front, which is a common place for the development of convective systems

353 (Laing and Fritsch 2000). Here, warm air advection is one of the forcing terms for ascent in

354 the quasi-geostrophic approximated ω-equation, and thus it is suggested that the hodograph

355 shape in Q is related with the large-scale ascent. Although other conditions (e.g., an intrusion

356 of jet in the upper troposphere) are required to induce the large-scale ascent, one possibility

357 for the existence of large-scale ascent is demonstrated from the hodograph.

358   Based on the analysis of the characteristics of the vertical profiles, the environmental

359 properties for the development of QSCCs will be described with the use of some stability

360 and shear indices that characterize environmental conditions in the following subsection. The

361 comparison between Q and N will also be provided.

362 *3.3. Diagnosis of conditions for the development of QSCCs with environmental*

363 *parameters*

364   As described in section 2.3, the environmental conditions for the development of QSCCs

365 are diagnosed in terms of stability and shear parameters. A diagnosis with the use of these

366 parameters is useful for identifying the differences of the environmental conditions between

367 Q and N.

368   Figure 13 shows the frequency distributions of the environmental parameters in Q and N.

369 To see general characteristics of the environmental parameters throughout Japan, all the data

370 shown in Figure 13 are composited for all the analysis sites. Except for TLR, the differences of

371 the parameters between Q and N are clearly seen. Compared to N, Q indicates a larger amount

372 of PW, a higher degree of instability (SSI, KI, and CAPE), and stronger shear (MS03) with a

373 larger hodograph curvature (EH03). Considering that there is a large difference of PW while

374 little difference of TLR between the categories, the moisture difference seems to control the

375 differences seen for other stability parameters as indicated by SSI (see Eq. (1) in Appendix),

376 KI (see Eq. (2) in Appendix), and CAPE.

377 From the analyses of vertical profiles of moisture, it was found that the moisture is larger in

378 Q than in N throughout the troposphere. Considering that SSI, KI, and CAPE become larger

379 with a larger amount of moisture content in the lower troposphere and that temperature lapse

380 rate was indicated to be near saturated neutral (moist adiabatic), it is suggested that the amount

381 of moisture in the lower layer controls the stability condition for the QSCCs.

382 [Figure 13 about here.]

383 Table 1 summarizes the averages and standard deviations of those environmental

384 parameters[3]. Statistical significance of the differences of the mean values between Q and

385 N is examined with the test statistic T. Table 1 also shows the values of test statistic T for

386 the environmental parameters. As expected from the features seen in Figure 13, it is found

387 that all the environmental parameters except TLR indicate a significant difference between

388 Q and N. Overall the T values pronouncedly exceed the significance level, and the T values

389 for PW and KI are the highest ones among the parameters. Because KI takes into account

390 the effects of moisture at the levels of 850 and 700 hPa (see Eq. (2) in Appendix), the higher

---

[3]To see the values of CAPE, PW, SSI, and MS03 for the QSCCs at all the sites and all the seasons, please see Tables SI-1–SI-4 of Supporting Information.

391 value of T in KI seems to be due to the significant difference of PW that may also affect

392 moisture at each vertical level. Therefore, the difference of the water vapor contents between

393 Q and N is considered to control the environmental properties for the development of QSCCs

394 rather than the difference of temperature lapse rate. The moisture content at each height will

395 be discussed later in this subsection. As far as the kinematic parameters are concerned, both

396 MS03 and EH03 indicate that there are significant differences between the categories. Thus,

397 the magnitude and direction of wind shear in the lower troposphere also characterize the

398 difference between Q and N.

399 [Table 1 about here.]

400 The distributions of CAPE, PW, and MS03, whose values are averaged during the warm

401 season at each site, are shown in Figure 14 in order to see the regional features of

402 environmental parameters. CAPE, PW, and MS03 are selected to examine stability, moisture,

403 and shear conditions, respectively. The values of CAPE and PW mostly increase with the

404 decrease in the latitude. The regional feature of CAPE is consistent with the previous findings

405 of Chuda and Niino (2005). In contrast, the values of MS03 are larger in the Hokkaido region

406 and in the southern part of Japan (SNM and KGS) ($> 13.0 \times 10^{-4}$ s^{-1}) than in the middle

407 of Japan (TTN, HMT, MTE, YNG, and FKO) ($< 13.0 \times 10^{-4}$ s^{-1}). Compared with Figure 6,

408 larger populations of QSCCs are mostly seen at locations with the larger values of CAPE and

409 PW.

410 [Figure 14 about here.]

411 The seasonal and regional variations of the environmental parameters are further described

412 here. Because of the significant differences between Q and N, the variations of the

413 environmental conditions for QSCCs are examined by concentrating on PW and KI.

414 Figure 15(a)–(c) shows the variation of the monthly mean PW and Figure 15(d)–(f) the

415 monthly mean KI. Each panel in Figure 15 summarizes the variations for each region. Both

416 PW and KI unanimously indicate higher values in Q than in N at all the locations in all the

417 months. In other words, the significant differences found in the overall averages shown in

418 Table 1 are consistently seen throughout the regions during the warm season. The variations

419 of PW and KI during the months show that highest values are generally seen in July and

420 August in Q. The PW and KI values take lowest values in May and October.

421   [Figure 15 about here.]

422 The results described above show that the moisture content is the most distinguishing factor

423 in characterizing the environmental conditions for the development of QSCCs from no-rain

424 cases among the stability parameters. Although PW is found to be an important parameter,

425 the levels at which moisture content contributes to PW are not known. Because it was found

426 that middle-level humidity plays important roles in controlling the structure and intensity of

427 cumulus convection and MCSs (Takemi *et al.* 2004; Derbyshire *et al.* 2004; Takemi 2007a;

428 Takemi 2014b; Takemi 2015), the moisture content at each vertical layer and its contribution

429 to the total amount of moisture (i.e., PW) are examined here. For this purpose, the vertically

430 integrated water vapor contents in vertical layers of a 1 km depth are computed. The vertically

431 integrated water vapor contents from the height of X km to Y km are referred to as PW

432 followed by the bottom (X km) and top (Y km) heights; for example, the water vapor content

433 vertically integrated from 0 to 1 km is referred to as PW01.

434   The differences of the layer-integrated moisture content between Q and N are compared in

435 terms of frequency distribution. The moisture content in all the layers is consistently larger in

436 Q than in N (not shown). In addition, the difference between the categories appears to be more

437 pronounced with the increase in the height level. This result indicates that the environmental

438 conditions for QSCCs are characterized by a larger amount of moisture at middle levels.

439   The importance of middle-level moisture content can also be found for the difference of the

440 contribution of the layer-integrated moisture to the total amount of moisture, i.e., PW. Thus,

441 we examined the contribution of the layer-integrated moisture content at each layer to PW

442 (Figure 16). Compared with the difference of the frequency distributions between Q and N

443 in the lower layers, the departure of the distribution in Q becomes more distinct from the N

444 distribution with the increase in the layer height. Namely, the amount of moisture at middle

445 levels largely contributes to precipitable water vapor in the environments of Q. Considering

446 that PW is significantly larger in Q than in N, it is suggested that an increase in the middle-level

447 moisture leads to a larger amount of PW for the development of the QSCCs.

448   The environmental condition with a larger amount of middle-level moisture was also

449 identified for convective precipitation events in the afternoon during the summer over the plain

450 regions (the metropolitan areas of Tokyo and Nagoya) facing to the Pacific in Japan (Nomura

451 and Takemi 2011; Takemi 2014a). The present analysis is consistent with these previous

452 findings. Therefore, a larger amount of moisture is considered to a common feature that

453 distinguishes the environments for the development of not only summertime thunderstorms

454 but also organized convective systems during the warm season in Japan. One thing to be

455 noted here is that, a larger middle-level moisture controls the convective development over

456 the tropics (Takemi *et al.* 2004; Kikuchi and Takayabu 2004), and the western part of Kyushu

457 Island (Kato 2006). At the mature stage of the quasi-stationary convective systems, the

458 moisture at the middle-level controls the development associated with the convective systems

459 (Kato 2006): the wet (dry) environment at the middle-level troposphere gives a condition

460 favorable (unfavorable) for the development of convective systems. Considering that the

461 larger middle-level moisture controls the development of convection, it is emphasized that

462 atmospheric moistening before the development stage of convection plays an important role

463 in the development of the QSCCs.

464 [Figure 16 about here.]

3.4. Relationships between environmental conditions and rainfall characteristics

466 In the previous subsection, the environmental properties for the development of the QSCCs

467 were investigated through the comparison of those in the no-rain cases. Differences in

468 the environmental properties between the QSCC occurrence and the no-rain cases were

469 demonstrated. In this subsection, the dependence of the intensity and area of rainfall produced

470 by QSCCs on the environmental conditions is investigated.

471 Figure 17 shows the relationships between the averaged precipitation intensity within the

472 identified QSCCs and the environmental parameters. The correlation coefficients between

473 the precipitation intensity and the parameters are also indicated. Although the correlation

474 coefficients are small, positive (negative) relationships of the precipitation intensity with the

Copyright © 2013 Royal Meteorological Society

Q. J. R. Meteorol. Soc. **00**: 2–39 (2013)

475 thermodynamic parameters are found for CAPE, CIN, and TLR (SSI). The relationships

476 between the precipitation intensity and the parameters CAPE, SSI, and TLR are reasonable,

477 because stronger instability is related to stronger precipitation intensity. For the shear

478 parameters (i.e., MS03 and EH03), there are negative relationships between the precipitation

479 intensity and the parameters. In terms of the correlation coefficient, the relationships of the

480 precipitation intensity with CAPE, SSI, TLR, and MS03 indicate higher correlation.

481 The relationships between the precipitation area of the QSCCs and the environmental

482 parameters are demonstrated in Figure 18. In contrast to the case of the precipitation intensity,

483 the relationships between the precipitation area and the thermodynamic parameters seem to

484 be inconsistent with convective instability concept. In general, the correlation coefficients

485 between the precipitation area and the thermodynamic parameters are negligible. On the other

486 hand, the relationships with the shear parameters indicate that there is a positive and higher

487 correlation of the precipitation area with the shear parameters. The highest correlation is seen

488 for the relationship with MS03.

489 From this analysis on the relationship between the precipitation characteristics and the

490 environmental parameters, it is found that higher convective instability is related to stronger

491 precipitation intensity while stronger vertical shear to larger precipitation area. Therefore,

492 it can be stated that convective instability has the strongest correlation with precipitation

493 intensity within the QSCCs and shear intensity is associated with the size of the precipitation

494 area.

495 [Figure 17 about here.]

496   [Figure 18 about here.]

3.5. *Characteristics of slower- and faster-moving systems*

498   In this study, we have focused on convective clusters whose motion speed is less than or

499   equal to 10 m s^{-1}, which we regard as quasi-stationary. However, the speed of about 10 m s^{-1}

500   may not be small; for example, Barnes and Sieckman (1984) termed a mesoscale convective

501   cloud line whose motion speed is greater than 7 m s^{-1} as a fast-moving line. Thus, in this

502   subsection, we examine and compare the characteristics between slower-moving and faster-

503   moving CCs.

504   Figure 19 shows the frequency distribution of the motion speed of the extracted QSCCs.

505   A peak frequency is found at the speed of 6.0 m s^{-1}, and the mean speed, v_{mean}, is 5.6 m

506   s^{-1}, indicating that the shape of the frequency distribution looks normal despite a little shift

507   to higher values. Thus, we divide the QSCCs into two sub-categories: slower-moving and

508   faster-moving CCs depending on their motion speed in order to show the differences in the

509   characteristics between slower-moving and faster-moving CCs. Slower-moving CCs (denoted

510   as S) are defined as clusters whose motion speed is less than $v_{\mathrm{mean}} - 1\sigma$, while faster-moving

511   CCs (denoted as F) as clusters whose motion speed is greater than $v_{\mathrm{mean}} + 1\sigma$, where standard

512   deviation of the motion speed of the extracted QSCCs, σ, is 1.8 m s^{-1}. Hereafter, the S and

513   F categories are referred to as S and F. Here, the total numbers of S and F are 706 and 718

514   among the 4,133 QSCCs, respectively.

515   [Figure 19 about here.]

516 Firstly, the statistics of the temporal and spatial means of precipitation intensity and the

517 temporal mean of precipitation area for each category are shown in Figure 20. Figure 20 shows

518 the maxima/minima, medians, and 75 and 25 percentiles. Precipitation intensity is larger in S

519 than in F (Figure 20(a)), while precipitation area is smaller in S than in F (Figure 20(b)).

520 The examination of the statistical significance of the differences in the means between the

521 two categories indicates that precipitation intensity is significantly larger in S than in F, while

522 precipitation area is significantly smaller in S than in F at the 95% confidence level. Therefore,

523 it is found that the slower-moving CCs have a stronger intensity and a smaller horizontal size

524 of precipitation than the faster-moving CCs.

525 [Figure 20 about here.]

526 To see how the difference of the distributions in Figure 20 arises from a viewpoint of the

527 environmental properties, Figure 21 compares the frequency distributions of the environmental

528 parameters in S and F. Compared to F, S indicates a smaller amount of PW, a higher degree

529 of instability (SSI, TLR, and CAPE), and weaker shear (MS03) with a smaller hodograph

530 curvature (EH03).

531 [Figure 21 about here.]

532 Statistical significance of the differences of the mean values between S and F is examined

533 with the test statistic T. Table 2 shows the values of test statistic T for the environmental

534 parameters. All the environmental parameters indicate statistically significant differences

535 between S and F. It is seen that the S environment shows higher instability (SSI, TLR, and

536 CAPE) and weaker shear (MS03 and EH03), but lower moisture (PW) than the F environment.

[Table 2 about here.]

The monthly changes of CAPE, PW, and MS03, respectively, are shown in Figure 22 with the same reason as described in section 3.3 and shown in Figure 14. CAPE (MS03) is clearly larger (smaller) in S than in F, in a consistent manner with those shown in Figure 21 and Table 2, while PW has a larger monthly variation in F than in S. Thus, it is suggested that there are no consistent features in the PW variation on the monthly basis.

We will describe again the relationships between environmental conditions and rainfall characteristics, but for S and F. Overall features for the precipitation intensity between S and F are the same as those between Q and N. This suggests that the environmental conditions for the slower-moving CCs are characterized by higher instability and weaker vertical shear. In contrast to the precipitation intensity, there are no discernible relationships between precipitation area and the environmental parameters (not shown).

[Figure 22 about here.]

From the analyses of environmental parameters for S and F, the physical interpretation of the results of Figures 20 and 21 are attempted here. Firstly, from the analyses of the relationships between environmental conditions and rainfall characteristics, it was found that the larger precipitation intensity is related to higher instability and to weaker shear intensity. The bulk Richardson number in S, estimated by using CAPE and a shear between the levels of 0 and 6 km (Table 2), is about 100, which corresponds to a condition for the development of multicell storms (Weisman and Klemp 1982). Because the CAPE values for Q are considerably smaller than those for squall lines and supercell storms over the Great Plains of the United States

558 (Bluestein and Jain 1985), stronger shears are detrimental to the development of convection

559 even in the multicell category in terms of bulk Richardson number. Thus, the moderate value

560 of the vertical wind shear is appropriate for the development of the slower-moving CCs, a type

561 of multicell storms, in Japan.

562 It is noted that the smaller precipitation area in the slower-moving CCs associated with

563 smaller MS03 can be attributed to the fact that the shape of shear determines the organization

564 mode of MCSs (LeMone *et al.* 1998; Parker and Johnson 2000). A stronger environmental

565 shear is in general favorable for a more organized structure on MCSs (e.g., Weisman and

566 Rotunno 2004). In addition, the environmental shear also restricts the size and motion of

567 convective cells within MCSs (e.g., Doswell *et al.* 1996). In other words, a weaker shear is

568 detrimental for the organization of convection. Therefore, it is considered that a weaker shear

569 condition identified for the slower-moving CCs leads to less organized and smaller CCs.

4. Summary and conclusions

571 The characteristics and environmental properties of QSCCs during the warm season in Japan

572 were statistically investigated using weather radar and upper-air sounding data of JMA from

573 May to October during 2005–2012. An algorithm developed by Shimizu and Uyeda (2012),

574 called AITCC, was modified to identify QSCCs from radar data. We found 4,133 QSCCs over

575 the Japanese major islands.

576 Compiling numerous QSCC samples revealed that the horizontal scales of QSCCs on

577 average and at the maximum with a circular shape are about 20 km and 72 km, respectively.

578 Thus, QSCCs in Japan are regarded as meso-β-scale phenomena. Ninety-five percent of

579 the extracted QSCCs have a lifetime of less than 60 minutes, and the number of longer-

580 lived QSCCs rapidly decreases as the lifetime increases. QSCCs occur more frequently

581 on the Pacific side of the Japanese islands and the inland regions in central Japan, which

582 are associated with higher convective instabilities, more moisture, and intermediate shear

583 intensities.

584 The analyses of the vertical profiles of temperature, water vapor mixing ratio, and horizontal

585 winds between the QSCC case and no-rain case indicate that the temperatures below the 850-

586 hPa level and above the 400-hPa level are larger in the QSCC case than in the no-rain case. It

587 is also indicated that the moisture content throughout the troposphere is larger in the QSCC

588 case than in the no-rain case. The shear profile indicates that there are pronounced differences

589 in the meridional component between the QSCC and the no-rain cases; there is a southerly

590 component in the QSCC cases and a northerly component in the no-rain cases, suggesting that

591 the hodograph shape in the QSCC cases is related with the large-scale ascent. Although other

592 conditions (e.g., an intrusion of the jet in the upper atmosphere) are required to induce the

593 large-scale ascent, one possibility for the existence of the large-scale ascent is demonstrated

594 in this study.

595 The environmental conditions for the occurrence of the QSCCs were further investigated

596 using stability and shear parameters. Most of the examined thermodynamic parameters

597 indicate that there is a significant difference in the stability condition of the QSCC and no-

598 rain cases. The moisture contents not only at the lower levels but also at the middle levels

599 (above the 2-km height) are significantly larger in the QSCC condition than in the no-rain

600 condition. This moisture difference leads to differences in KI, SSI, and PW between the QSCC

and no-rain cases. The kinematic parameters indicated that both MS03 and EH03 significantly characterize the environmental conditions of the QSCC cases from the no-rain cases. From the diagnosis using the environmental indices, it is concluded that the amount of moisture in the lower layer controls the stability condition for the development of the QSCCs, and that the magnitudes of the wind shear and the helicity at the lower levels distinguish the kinematic environment for the development of the QSCCs.

In addition, the moisture content at each vertical level and its contribution to the total amount of moisture (i.e., PW) were also examined. An increase in the middle-level moisture leads to more PW in the QSCC environments. Considering that a larger middle-level moisture controls the development of convection (Takemi *et al.* 2004; Kikuchi and Takayabu 2004; Derbyshire *et al.* 2004; Kato 2006; Takemi 2015), atmospheric moistening before the development stage of convection plays an important role in the development of the QSCCs.

Examining the relationship between the precipitation intensity/area of the QSCCs and the environmental parameters shows that the precipitation intensity is more strongly correlated with CAPE and SSI, while the precipitation area is more highly correlated with MS03. Simply stated, the statistical analyses of numerous QSCCs samples extracted from the long-term data reveal that the precipitation intensity within the QSCCs during the warm season in Japan has a higher correlation with the convective instability while the precipitation area has a stronger correlation with the shear intensity.

The characteristics and environmental properties between slower- and faster-moving CCs were compared. Investigating the statistical significance of the differences in the means between the two categories indicates that the precipitation intensity is significantly larger in

slower-moving CCs than in faster-moving CCs, while the precipitation area is significantly smaller in the slower-moving CCs. The analysis of environmental parameters suggests that the stronger precipitation intensity for the slower-moving CCs is due to a higher instability and a weaker shear intensity, whereas the smaller precipitation area is due to a weaker shear intensity.

QSCCs are widespread mesoscale phenomena not only in Japan but also around the world. In generating QSCCs, a complex topography should play an important role. A complex terrain characterizes the geographical features in Japan; and therefore the geographical features should have a significant impact on the occurrence of QSCCs. In addition, moister conditions characterize the environmental settings for the occurrence of QSCCs in humid-climate regions. From the numerical experiments conducted by Takemi (2014b), moister environments lead to the development of stronger and more organized CCs. The present study shows that middle-level moister conditions favor the occurrence of stronger precipitation intensity within the QSCCs. These results should contribute to the understanding of quasi-stationary or slow-moving convective clusters in those regions.

Furthermore, the present study demonstrates that operational data such as radars, upper-air soundings, and high-resolution gridded analyses provided by meteorological centers are very useful for investigating mesoscale convective phenomena and their environmental properties from a climatological point of view. Although we have previously conducted this type of study using operational meteorological data (Nomura and Takemi 2011; Takemi 2014a), the present study also confirms the usefulness of this approach. The outcome from our studies should provide basic information on the diagnosis of mesoscale phenomena.

Acknowledgements

Appendix: Definition of SSI and KI

To assist the discussion on the relationships between the thermodynamic-vertical profiles and environmental properties in the sections from 3.2 to 3.5, we will describe the definition of Showalter Stability Index (SSI) and K Index (KI) as follows;

$$SSI = T_{500} - T^*_{850 \to 500}, \tag{1}$$

$$KI = T_{850} - T_{500} + T_{d850} - (T_{700} - T_{d700}), \tag{2}$$

where T_{850}, T_{700}, and T_{500} are the temperature at the 850, 700, and 500 hPa level, respectively. T_{d850} and T_{d700} are the dew-point temperature at the 850 hPa and 700 hPa, respectively, and

663 $T^*_{850 \to 500}$ is the 500-hPa temperature whose property is adiabatically lifted from 850 hPa to

664 500 hPa.

References

666 Anquetin S, Minsicloux F, Creutin JD, Cosma S. 2003. Numerical simulation of orographic

667 rainbands. *J. Geophys. Res.*, **108:** D88386, DOI: `10.1029/2002JD001593`.

668 Barnes GM, Sieckman K. 1984. The environment of fast- and slow-moving trop-

669 ical mesoscale convective cloud lines. *Mon. Wea. Rev.*, **112:** 1782–1794, DOI:

670 `10.1175/1520-0493(1984)112<1782:TEOFAS>2.0.CO;2`.

671 Bluestein HB, Jain MH. 1985. Formation of mesoscale lines of precipitation: Severe

672 squall lines in Oklahoma during the spring. *J. Atmos. Sci.*, **42:** 1711–1732, DOI:

673 `10.1175/1520-0493(1987)115<2719:FOMLOP>2.0.CO;2`.

674 Buzzi A, Foschini L. 2000. Mesoscale meteorological features associated with heavy

675 precipitation in the Southern Alpine region. *Meteorol. Atmos. Phys.*, **72:** 131–146, DOI:

676 `10.1007/s007030050011`.

677 Chappell CF. 1986. Quasi-stationary convective events. In *Mesoscale Meteorology and*

678 *Forecasting*. Ray PS. (ed.) 289–310. Amer. Meteorol. Soc: Boston, MA.

679 Chuda T, Niino H. 2005. Climatology of environmental parameters for mesoscale convections

680 in Japan. *J. Meteor. Soc. Jpn*, **83:** 391–408, DOI: `10.2151/jmsj.83.391`.

681 Davolio S, Buzzi A, Malguzzi P. 2009. Orographic triggering of long lived

682 convection in three dimensions. *Meteorol. Atmos. Phys.*, **103:** 35–44, DOI:

683 `10.1007/s00703-008-0332-5`.

684 Davies-Jones RP. 1984. Streamwise Vorticity: The origin of updraft

685 rotation in supercell storms. *J. Atmos. Sci.*, **41:** 2991–3006, DOI:

686 `10.1175/1520-0469(1984)041<2991:SVTOOU>2.0.CO;2`.

687 Derbyshire SH, Beau I, Bechtold P, Grandpeix JY, Piriou JM, Redelsperger JL, Soares PMM.

688 2004. Sensitivity of moist convection to environmental humidity. *Q. J. R. Meteorol. Soc.*,

689 **130:** 3055–3079, DOI: `10.1256/qj.03.130`.

690 Doswell CA, Brooks HE, Maddox RA. 1996. Flash flood forecasting:

691 An ingredients-based methodology. *Wea. Forecasting*, **11:** 560–581, DOI:

692 `10.1175/1520-0434(1996)011<0560:FFFAIB>2.0.CO;2`.

693 Geerts B. 1998. Mesoscale convective systems in the Southeast United

694 States during 1994–95: A survey. *Wea. Forecasting*, **13:** 860–869, DOI:

695 `10.1175/1520-0434(1998)013<0860:MCSITS>2.0.CO;2`.

696 George JJ. 1960. *Weather forecasting for aeronautics*. Academic Press: New York; pp. 673.

697 Glickman TS (ed). 2000. *Glossary of Meteorology*, 2nd edition. American Meteorological

698 Society: Boston; pp. 855.

699 Hirockawa Y, Kato T. 2012. Kinetic energy budget analysis on the development of a meso-β-

700 scale vortex causing heavy rainfall, observed over Aomori Prefecture in Northern Japan on

701 11 November 2007. *J. Meteor. Soc. Jpn*, **90:** 905–921, DOI: `10.2151/jmsj.2012-604`.

702 Kato T. 1998. Numerical simulation of the band-shaped torrential rain observed over Southern

703 Kyushu Japan on 1 August 1993. *J. Meteor. Soc. Jpn*, **76:** 97–128.

704 Kato T. 2005. Statistical study of band-shaped rainfall systems the Koshikijima and Nagasaki

705 lines observed around Kyushu Island Japan. *J. Meteor. Soc. Jpn*, **83:** 943–957, DOI:

706 10.2151/jmsj.83.943.

707 Kato T. 2006. Structure of the band-shaped precipitation system inducing the heavy rainfall

708 observed over northern Kyushu, Japan on 29 June 1999. *J. Meteor. Soc. Jpn*, **84:** 129–153,

709 DOI: 10.2151/jmsj.84.129.

710 Kato T, Aranami K. 2005. Formation factors of 2004 Niigata-Fukushima and Fukui heavy

711 rainfalls and problems in the predictions using a cloud-resolving model. *SOLA*, **1:** 1–4, DOI:

712 10.2151/sola.2005-001.

713 Kato T, Goda H. 2001. Formation and maintenance processes of a stationary band-shaped

714 heavy rainfall observed in Niigata on 4 August 1998. *J. Meteor. Soc. Jpn*, **79:** 899–924,

715 DOI: 10.2151/jmsj.79.899.

716 Kikuchi K, Takayabu YN. 2004. The development of organized convection associated with

717 the MJO during TOGA COARE IOP: Trimodal characteristics. *Geophys. Res. Lett.*, **31:**

718 L10101, DOI: 10.1029/2004GL019601.

719 Laing AG, Fritsch JM. 2000. The large-scale environments of the global popula-

720 tions of mesoscale convective complexes. *Mon. Wea. Rev.*, **128:** 2756–2776, DOI:

721 10.1175/1520-0493(2000)128<2756:TLSEOT>2.0.CO;2.

722 LeMone MA, Zipser EJ, Trier SB. 1998. The role of environmental shear and

723 thermodynamic conditions in determining the structure and evolution of mesoscale

724 convective systems during TOGA COARE. *J. Atmos. Sci.*, **55:** 3493–3519, DOI:

725 10.1175/1520-0469(1998)055<3493:TROESA>2.0.CO;2.

726 Maddox RA. 1980. Mesoscale convective complexes. *Bull. Amer. Meteor. Soc.*, **61:** 1374–

727 1387, DOI: 10.1175/1520-0477(1980)061<1374:MCC>2.0.CO;2.

728 Markowski P, Richardson Y. 2010. *Mesoscale meteorology in midlatitudes*. Wiley-Blackwell:

729 pp. 407.

730 Meng Z, Yan D, Zhang Y. 2013. General features of squall lines in East China. *Mon. Wea.*

731 *Rev.*, **141:** 1629–1647, DOI: 10.1175/MWR-D-12-00208.1.

732 Nomura S, Takemi T. 2011. Environmental stability for afternoon rain events in the Kanto

733 Plain in summer. *SOLA*, **7:** 9–12, DOI: 10.2151/sola.2011-003.

734 Ogura Y. 1991. Analysis and mechanism of intense precipitation. *Tenki*, **38:** 276–288 (in

735 Japanese).

736 Orlanski I. 1975. A rational subdivision of scales for atmospheric processes. *Bull. Am.*

737 *Meteorol. Soc.*, **56:** 527–530.

738 Panziera L, James CN, Germann U. 2014. Mesoscale organization and structure of orographic

739 precipitation producing flash floods in the Lago Maggiore region. *Q. J. R. Meteorol. Soc.*,

740 **141:** 224–248, DOI: 10.1002/qj.2351.

741 Parker MD, Johnson RH. 2000. Organizational Modes of Midlatitude

742 Mesoscale Convective Systems. *Mon. Wea. Rev.*, **128:** 3413–3436, DOI:

743 10.1175/1520-0493(2001)129<3413:OMOMMC>2.0.CO;2.

744 Rasmussen EN, Blanchard DO. 1998. A baseline climatology of sounding-derived

745 supercell and tornado forecast parameters. *Wea. Forecasting*, **13:** 1148–1164, DOI:

746 10.1175/1520-0434(1998)013<1148:ABCOSD>2.0.CO;2.

Schumacher RS, Johnson RH. 2008. Mesoscale processes contributing to extreme rainfall in a midlatitude warm-season flash flood. *Mon. Wea. Rev.*, **136:** 3964–3986, DOI: `10.1175/2008MWR2471.1`.

Shimizu S, Uyeda H. 2012. Algorithm for the identification and tracking of convective cells based on constant and adaptive threshold methods using a new cell-merging and -splitting scheme. *J. Meteor. Soc. Jpn*, **90:** 869–899, DOI: `10.2151/jmsj.2012-602`.

Steiner M, Houze RA, Yuter SE. 1995. Climatological characterization of three-dimensional storm structure from operational radar and rain gauge data. *J. Appl. Meteor.*, **34:** 1978–2007, DOI: `10.1175/1520-0450(1995)034<1978:CCOTDS>2.0.CO;2`.

Takemi T. 2007a. A sensitivity of squall line intensity to environmental static stability under various shear and moisture conditions. *Atmos. Res.*, **84:** 374–389, DOI: `10.1016/j.atmosres.2006.10.001`.

Takemi T. 2007b. Environmental stability control of the intensity of squall lines under low-level shear conditions. *J. Geophys. Res.*, **112:** D24110, DOI: `10.1029/2007JD008793`.

Takemi T. 2014a. Characteristics of summertime afternoon rainfall and its environmental conditions in and around the Nobi Plain. *SOLA*, **10:** 158–162, DOI: `10.2151/sola.2014-033`.

Takemi T. 2014b. Convection and precipitation under various stability and shear conditions: Squall lines in tropical versus midlatitude environment. *Atmos. Res.*, **142:** 111–123, DOI: `10.1016/j.atmosres.2013.07.010`.

Takemi T. 2015. Relationship between cumulus activity and environmental moisture during the CINDY2011/DYNAMO field experiment as revealed from convection-resolving simulations. *J. Meteor. Soc. Jpn*, in press, DOI: `10.2151/jmsj.2015-035`.

Takemi T, Hirayama O, Liu C. 2004. Factors responsible for the vertical development of tropical oceanic cumulus convection. *Geophys. Res. Lett.*, **31:** L11109, DOI: `10.1029/2004GL020225`.

Warren RA, Kirshbaum DJ, Plant RS, Lean HW. 2014. A 'Boscastle-type' quasi-stationary convective system over the UK Southwest Peninsula. *Q. J. R. Meteorol. Soc.*, **140:** 240–257, DOI: `10.1002/qj.2124`.

Weisman ML, Klemp JB. 1982. The dependence of numerically simulated convective storms on vertical wind shear and buoyancy. *Mon. Wea. Rev.*, **110:** 504–520, DOI: `10.1175/1520-0493(1982)110<0504:TDONSC>2.0.CO;2`.

Weisman ML, Rotunno R. 2004. "A Theory for Strong Long-Lived Squall Line" Revisited. *J. Atmos. Sci.*, **61:** 361–382, DOI: `10.1175/1520-0469(2004)061<0361:ATFSLS>2.0.CO;2`.

Yoshizaki M, Kato T. 2007. *Meteorology of heavy rainfall and snowfall*. Asakura Publishing Co.: pp. 187 (in Japanese).

Yoshizaki M, Kato T, Tanaka Y, Takayama H, Shoji Y, Seko H. 2000. Analytical and numerical study of the 26 June 1998 orographic rainband observed in Western Kyushu, Japan. *J. Meteor. Soc. Jpn*, **78:** 835–856.

List of Figures

Copyright © 2013 Royal Meteorological Society

Q. J. R. Meteorol. Soc. **00**: 2–39 (2013)
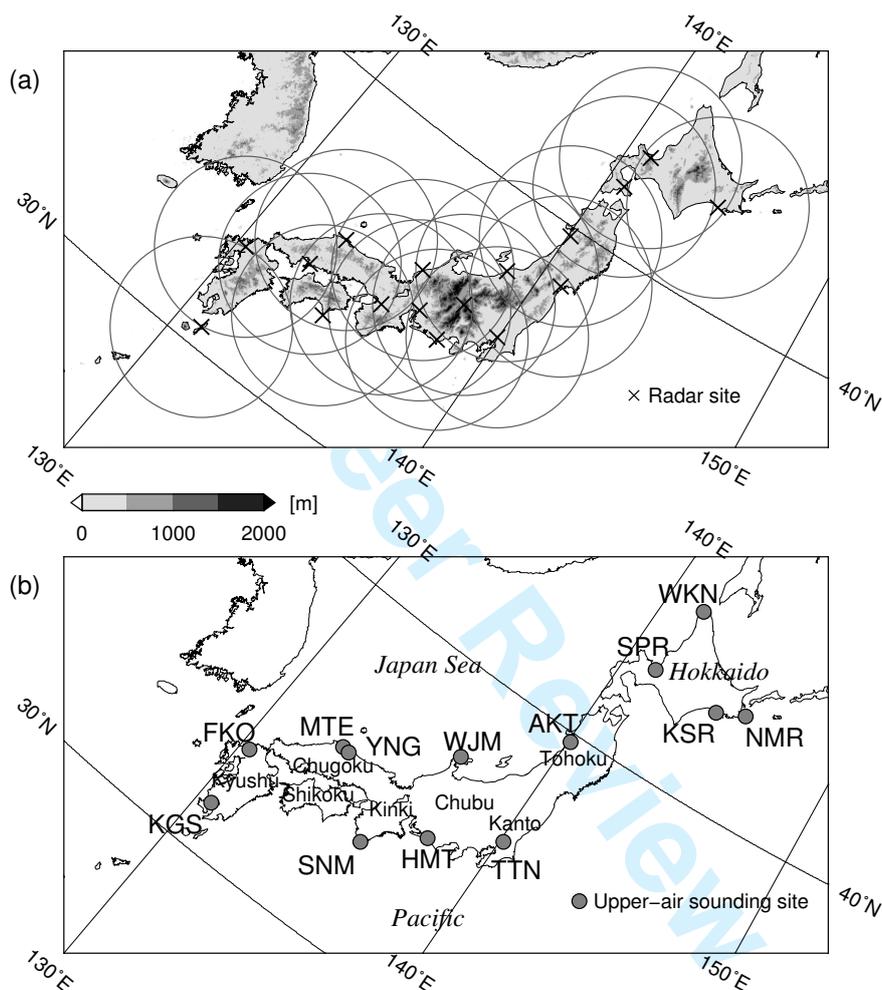
Prepared using qjrms4.cls

Figure 1. The locations of (a) the operational radar (indicated by crosses) and (b) the radiosonde sites (gray circles). In (a), the detecting ranges of the operational radar are displayed with solid circles, and the shade indicates surface elevation with the 500-m interval. See the texts for the acronyms of the radiosonde sites indicated in (b).
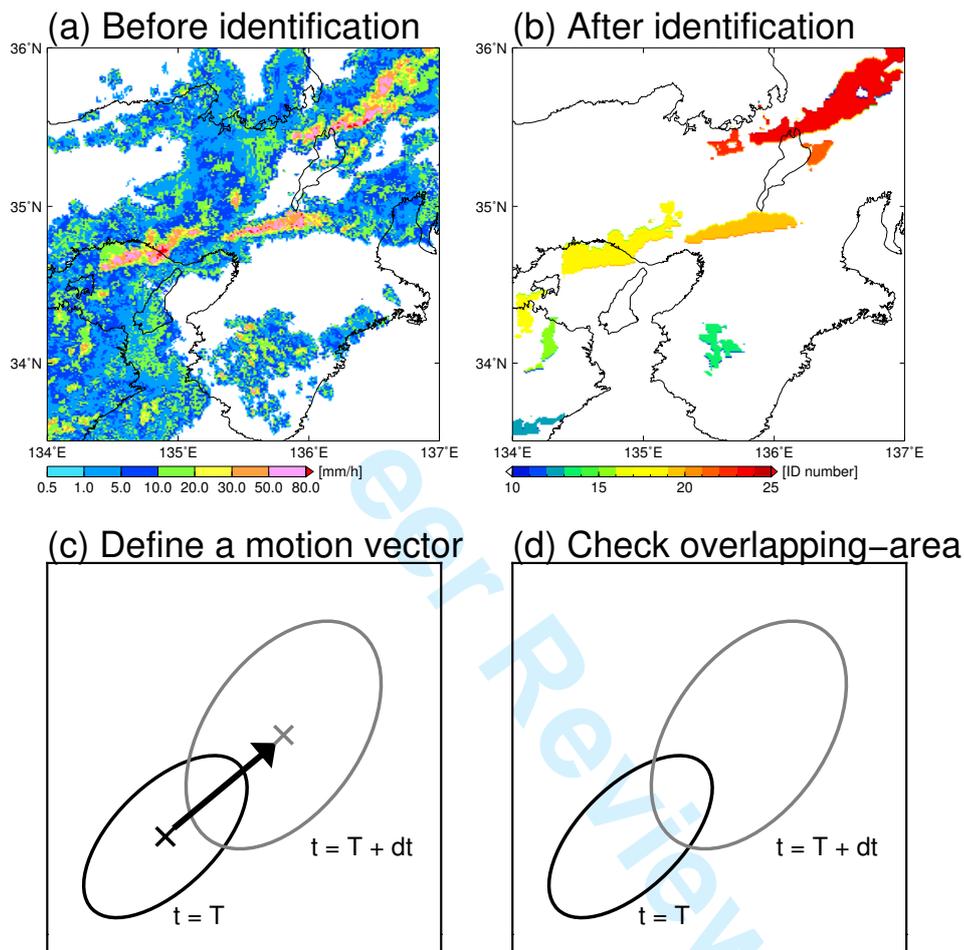
Copyright © 2013 Royal Meteorological Society

Q. J. R. Meteorol. Soc. **00**: 2–39 (2013)

Prepared using qjrms4.cls

Figure 2. The schematic procedures to extract QSCCs in this study. (a) An original distribution of precipitation intensity (mm h^{-1}) before identifying CCs. The threshold value of 10 mm h^{-1} is for the minimum precipitation intensity to determine a contiguous area of CCs. (b) A result of extracting CCs. Color indicates individual ID numbers for the CCs. (c) The motion vector in the tracking procedure. (d) The case where a part of the CC at t = T and a part of the CC at t = T + dt are overlapped.
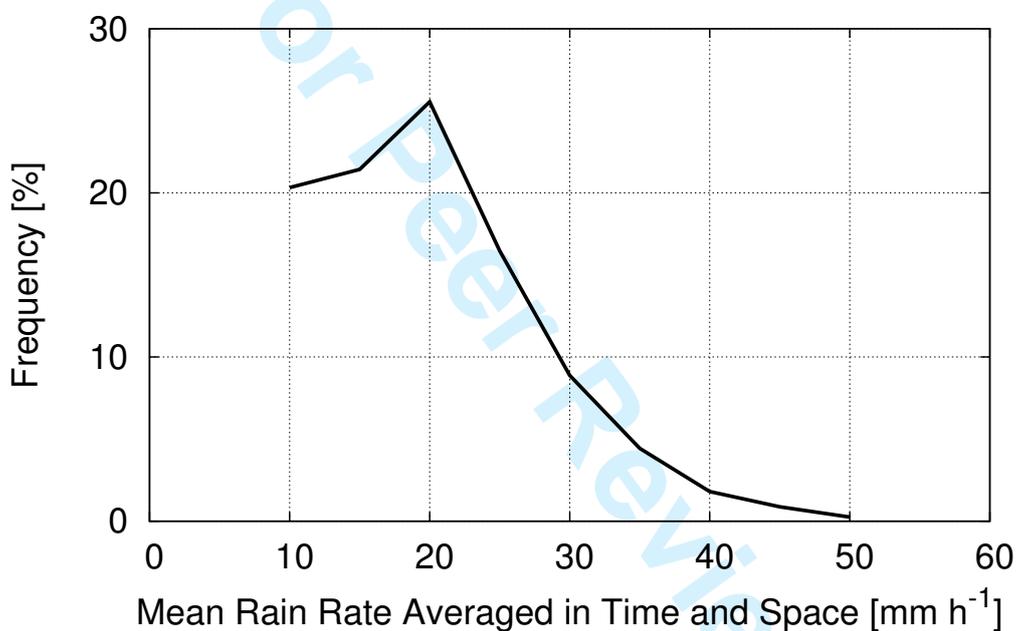
Figure 3. Frequency distribution of the time-mean precipitation intensity averaged for the lifetime of each QSCC, counted at the interval of 5 mm h^{-1}. The frequency at a rain rate r means the value accumulated over the rain rate between r-2.5 and r+2.5.
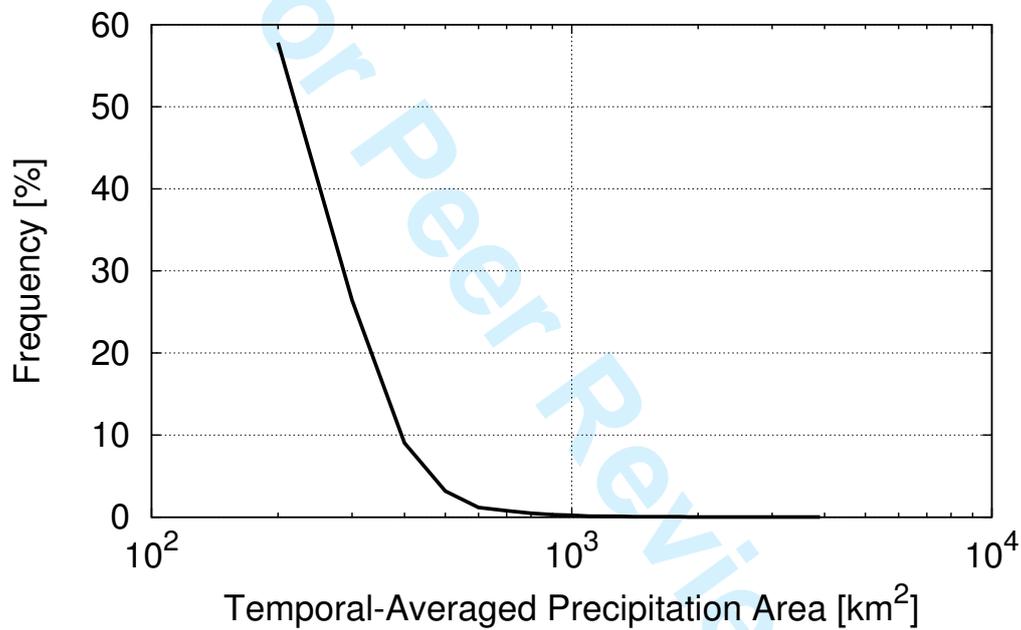
Q. J. R. Meteorol. Soc. **00**: 2–39 (2013)

Prepared using qjrms4.cls

Figure 4. The same as Figure 3, except for the time-averaged precipitation area for the QSCCs, accumulated at the interval of 100 km^2 and the range from a-50 to a+49, where a is a precipitation area.
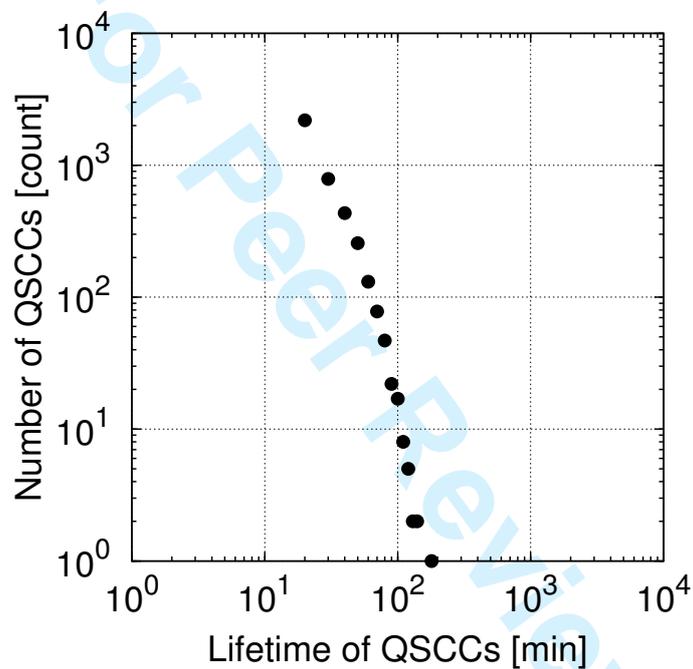
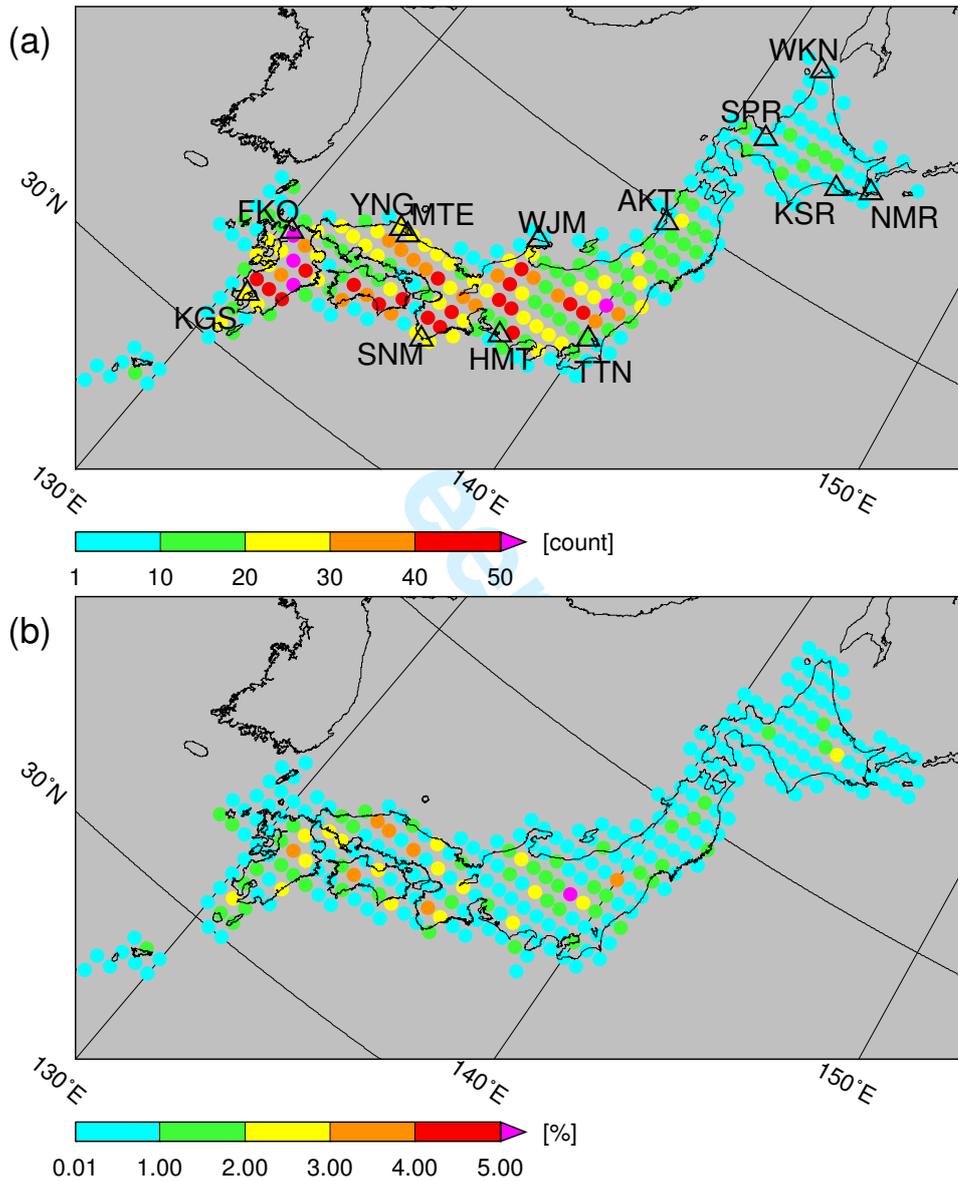**Figure 5.** Number of QSCCs with respect to their lifetimes, counted at the 10-minutes interval.

Copyright © 2013 Royal Meteorological Society

Q. J. R. Meteorol. Soc. **00**: 2–39 (2013)

Prepared using qjrms4.cls

1
2
3
4
5
6
7
8
9
10
11
12
13
14
15
16
17
18
19
20
21
22
23
24
25
26
27
28
29
30
31
32
33
34
35
36
37
38
39
40
41
42
43
44
45
46
47
48
49
50
51
52
53
54
55
56
57
58
59
60

Figure 6. (a) The frequency distribution of QSCCs that evaluated over the 50-km^2 area. (b) The same as (a) but the percentage of the rainfall that is produced by QSCCs to the total rainfall during the warm season. The locations of the radiosonde sites are indicated by triangles at (a).
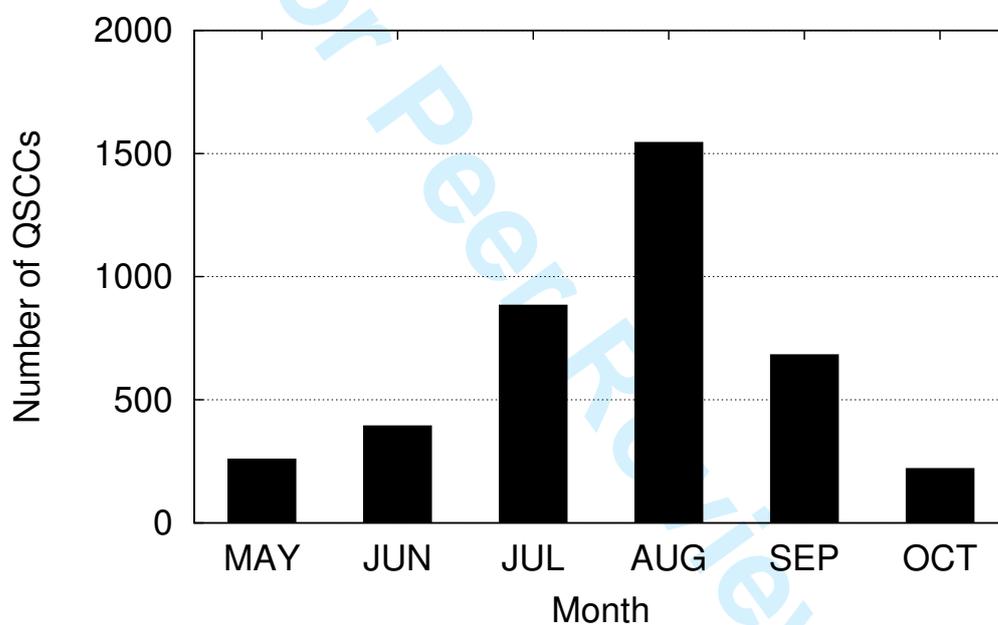
1
2
3
4
5
6
7
8
9
10
11
12
13
14
15
16
17
18
19
20
21
22
23
24
25
26
27
28
29
30
31
32
33
34
35
36
37
38
39
40
41
42
43
44
45
46
47
48
49
50
51
52
53
54
55
56
57
58
59
60

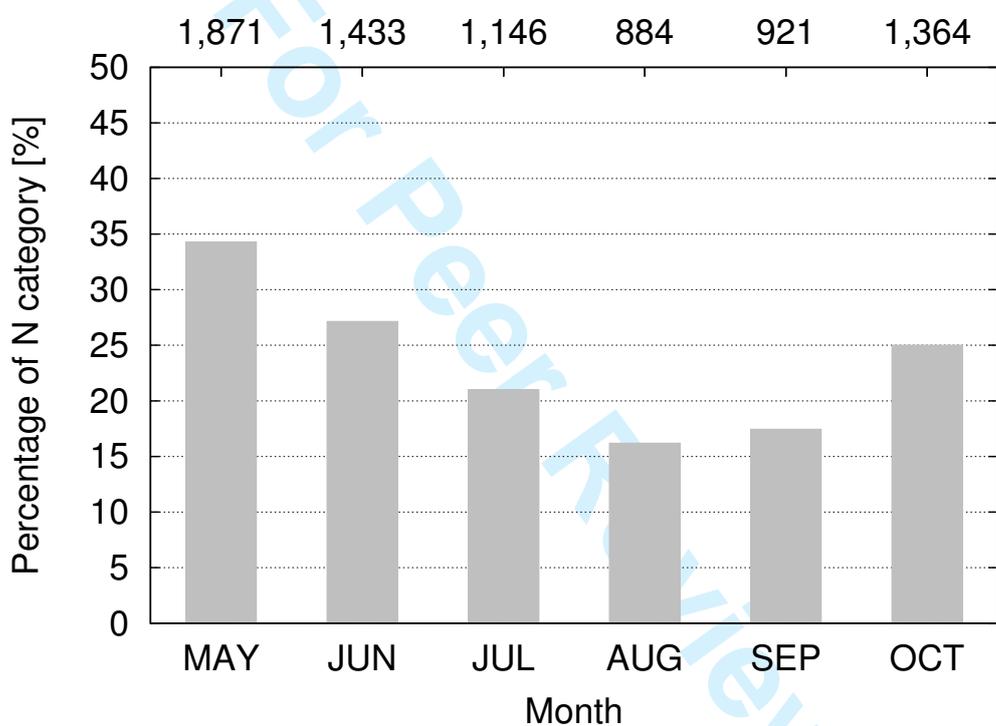**Figure 7.** Month-to-month change of the occurrence of QSCCs.

Figure 8. Percentage of the frequency of the no-rain cases (N category) to all the radiosonde observation times. Actual numbers of the N category are given on the upper horizontal axis.
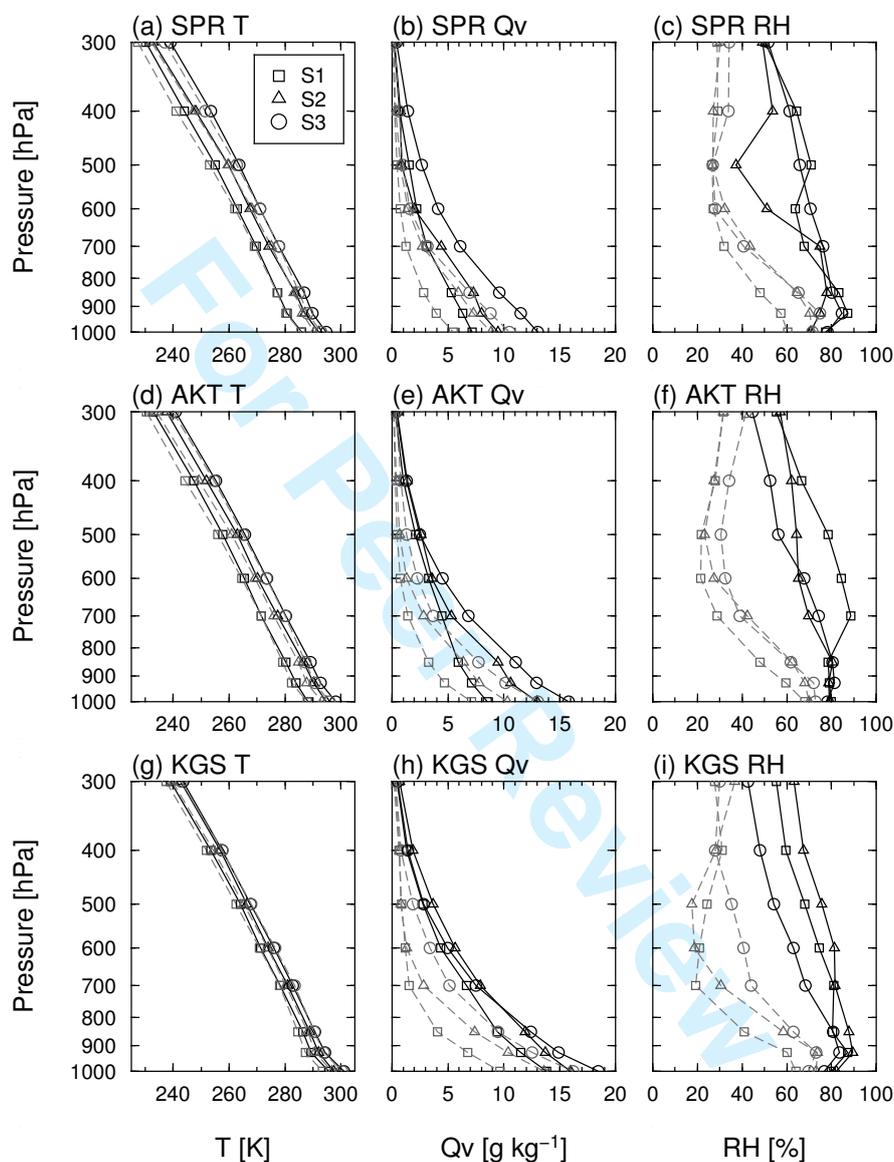
Copyright © 2013 Royal Meteorological Society

Q. J. R. Meteorol. Soc. **00**: 2–39 (2013)

Prepared using qjrms4.cls

Figure 9. The vertical profile of the mean temperature in (a) SPR, (d) AKT, and (g) KGS, the mean water vapor mixing ratio in (b) SPR, (e) AKT, and (h) KGS, and the relative humidity in (c) SPR, (f) AKT, and (i) KGS averaged from radiosonde observations in each site of QSCCs (Q, black solid line) and no-rain cases (N, gray dashed line). The rectangle, triangle, and circle show the profiles for S1 (May; Octorber), S2 (June), and S3 (July–September), respectively.
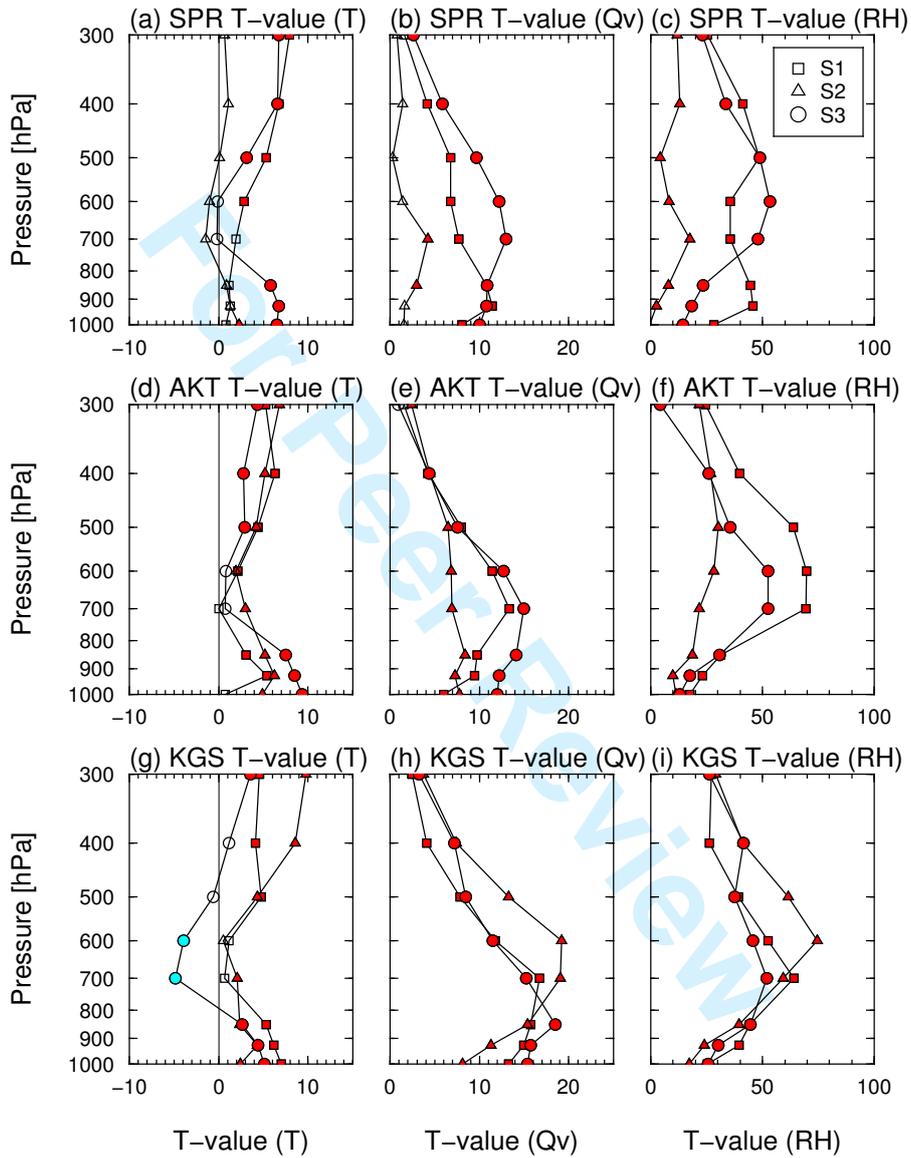
Copyright © 2013 Royal Meteorological Society

Q. J. R. Meteorol. Soc. **00**: 2–39 (2013)

Prepared using qjrms4.cls

Figure 10. The same as Figure 9, except for the T-values of the differences in the mean values between QSCCs (Q) and no-rain cases (N). The red and cyan marks indicate that the values are significantly different at the 95% confidence level.
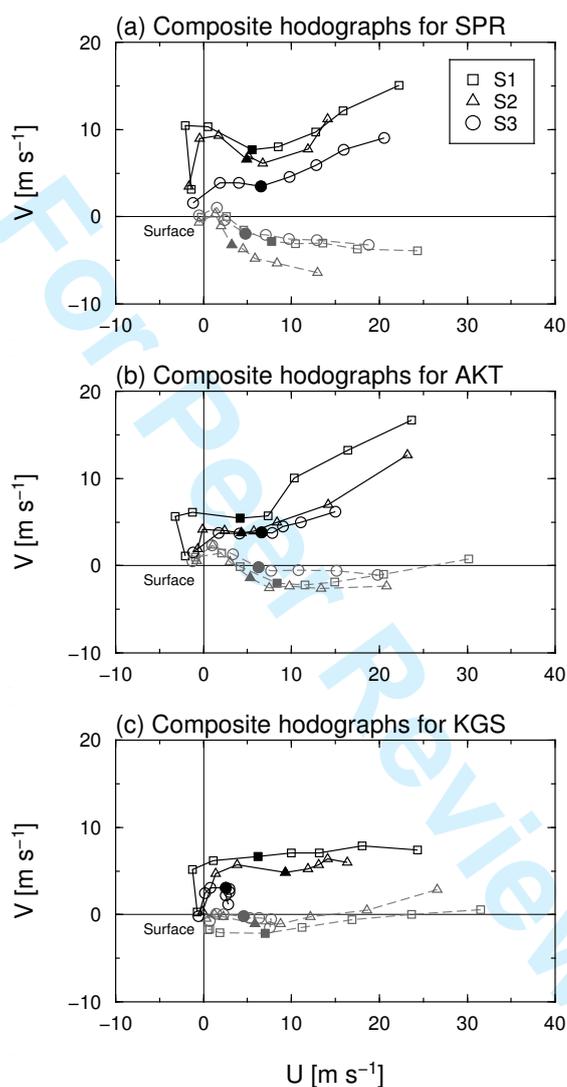
Figure 11. The mean wind hodograph in (a) SPR, (b) AKT, and (c) KGS averaged from radiosonde observations in each site of QSCCs (Q, black solid line) and no-rain cases (N, gray solid line). The rectangle, triangle, and circle indicate the hodographs for S1 (May; Octorber), S2 (June), and S3 (July–September). The filled marks indicate the wind at the 700-hPa level.
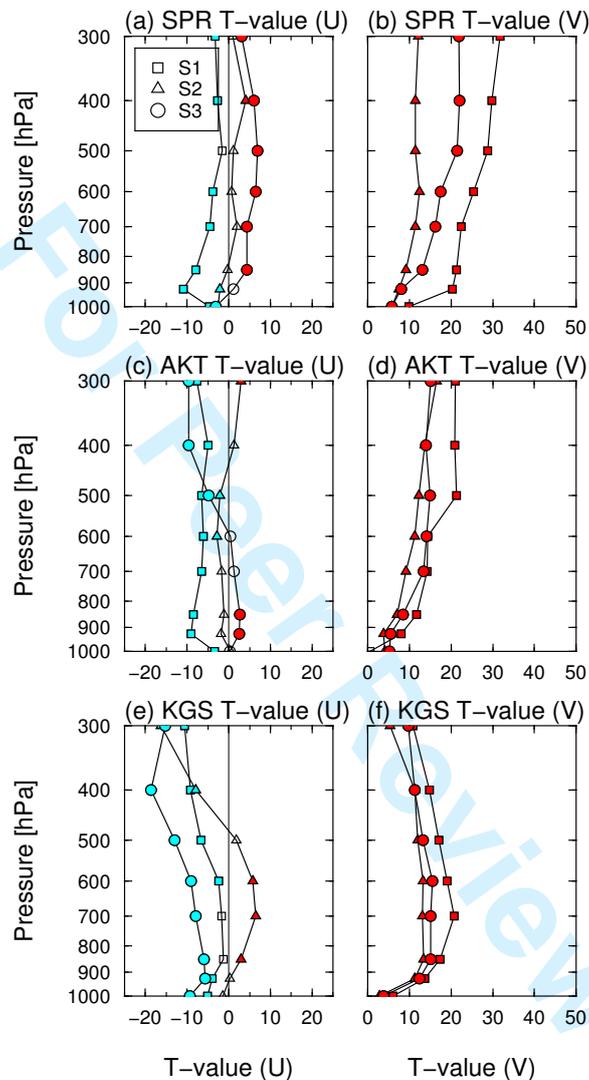
Copyright © 2013 Royal Meteorological Society

Q. J. R. Meteorol. Soc. **00**: 2–39 (2013)

Prepared using qjrms4.cls

Figure 12. The vertical profile of T-values of the differences in the mean values of (a) (c) (e) the zonal wind speed, and (b) (d) (f) the meridional wind speed between QSCCs (Q) and no-rain cases (N) for (a) (b) SPR, (c) (d) AKT, and (e) (f) KGS. The rectangle, triangle, and circle indicate the hodographs for S1 (May; Octorber), S2 (June), and S3 (July–September). The red and cyan marks indicate that the values are significantly different at the 95% confidence level.
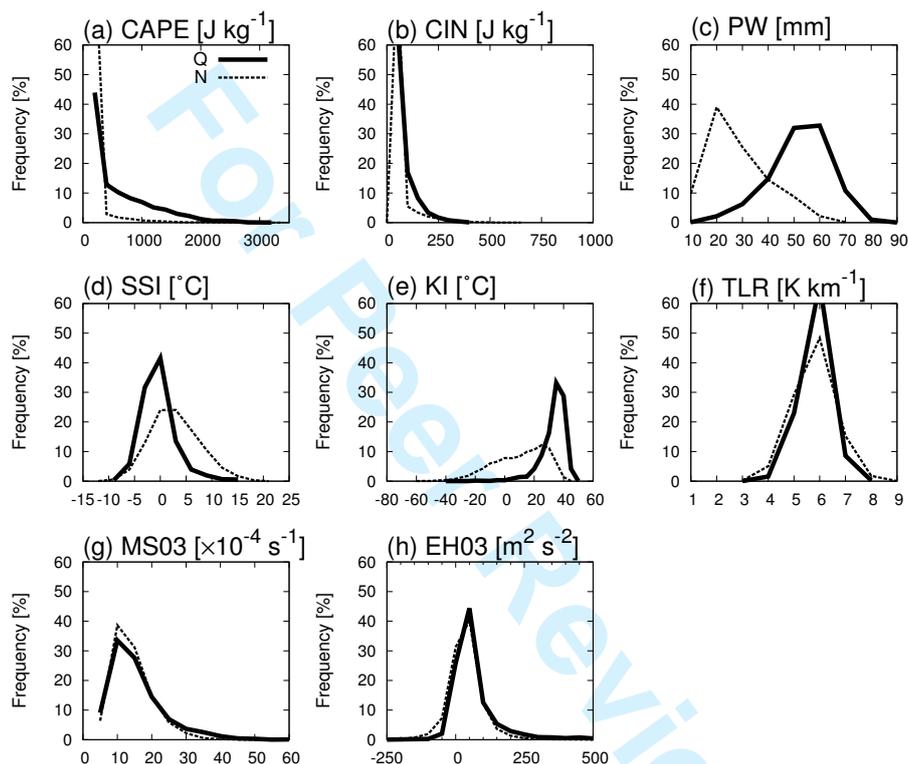
Figure 13. Frequency distributions of the environmental parameters calculated from radiosonde observations for QSCCs (Q) and no-rain cases (N). (a) CAPE [J kg^{-1}], (b) CIN [J kg^{-1}], (c) PW [mm], (d) SSI [°C], (e) KI [°C], (f) TLR [K km^{-1}], (g) MS03 [×10^{-4} s^{-1}], and (h) EH03 [m^2 s^{-2}]. Black solid line and gray dashed line indicate the values of Q and N, respectively. The frequency intervals in (a)–(h) are 200, 50, 10, 3, 5, 1, 5, and 50, respectively. The values show the frequencies that are accumulated at the center of the intervals.

Copyright © 2013 Royal Meteorological Society

Q. J. R. Meteorol. Soc. **00**: 2–39 (2013)

Prepared using qjrms4.cls

Figure 14. The distributions of the warm-season-mean environmental parameters of (a) CAPE, (b) PW, and (c) MS03 calculated from radiosonde observations for QSCCs.
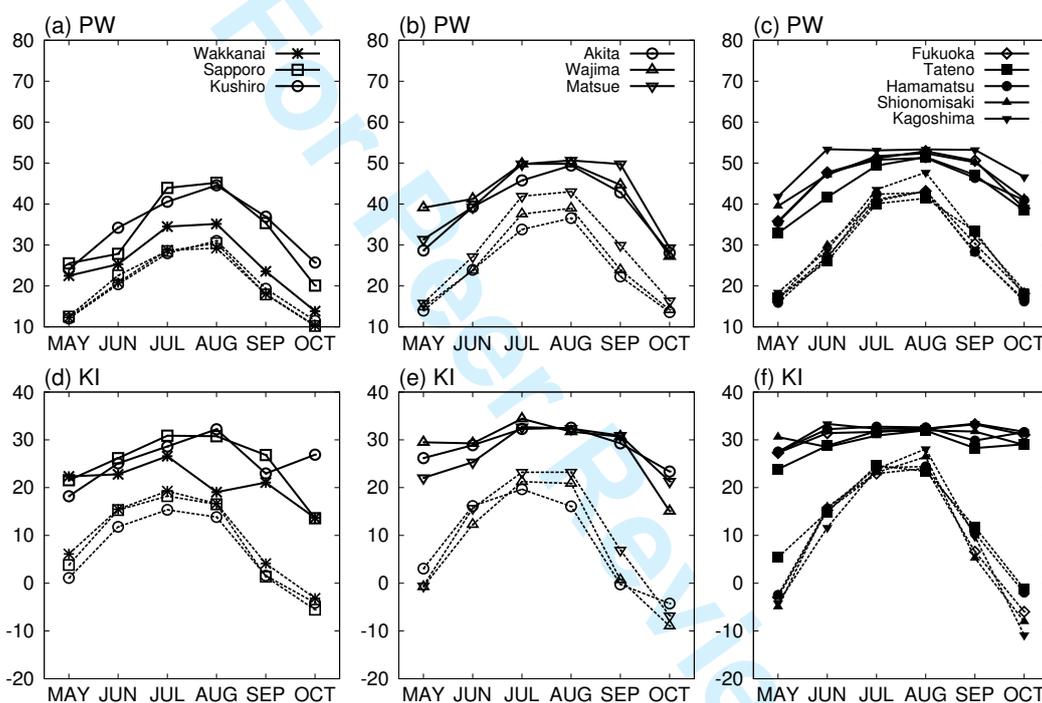
Figure 15. Monthly averages of the regional-mean environmental parameters calculated from radiosonde observations for QSCCs (Q) and no-rain cases (N): PW in (a)–(c); and KI in (d)–(f). Black solid line and gray dashed line indicate Q and N, respectively.
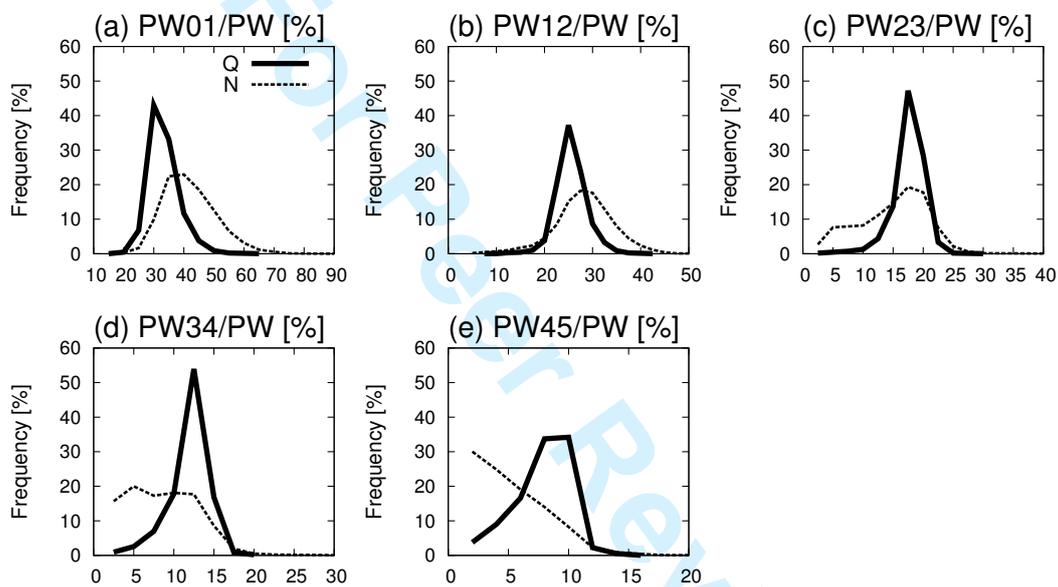
Figure 16. The percentage of the layer-integrated moisture content to the precipitable water in the layer of of (a) 0–1 km, (b) 1–2 km, (c) 2–3 km, (d) 3–4 km, and (e) 4–5 km of radiosonde observations (all 11 sites) for QSCCs (Q, solid line) and no-rain cases (N, dashed line). The frequency intervals in (a), (b)–(d), and (e) are 5, 2.5, and 2, respectively. The values show the frequencies that are accumulated at the center of the intervals.
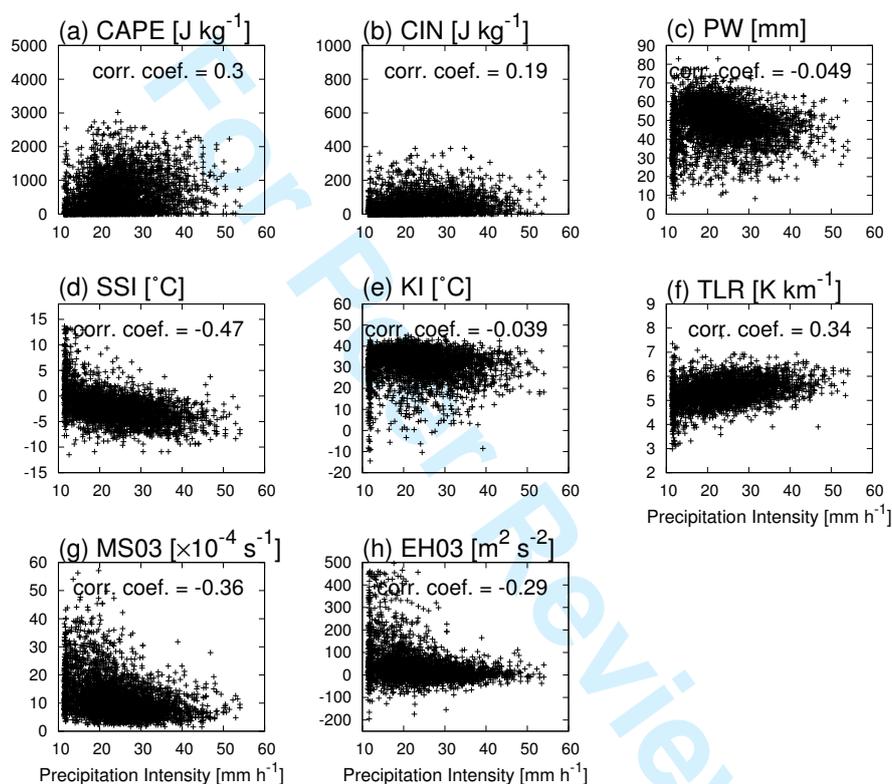
Figure 17. The relationships of the mean precipitation intensity averaged in time and space for the QSCCs with (a) CAPE, (b) CIN, (c) PW, (d) SSI, (e) KI, (f) TLR, (g) MS03, and (h) EH03. Correlation coefficients between the precipitation intensity and the environmental parameters were also given at the upper-right corner in each panel.
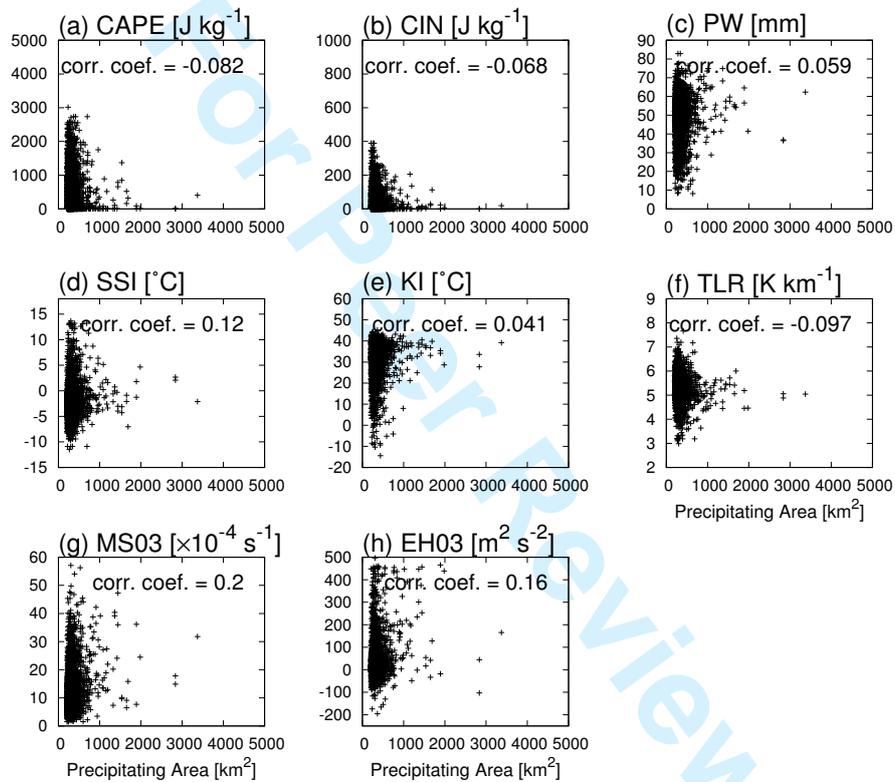
Figure 18. The same as Figure 17, except for the time-averaged precipitation area for the QSCCs.
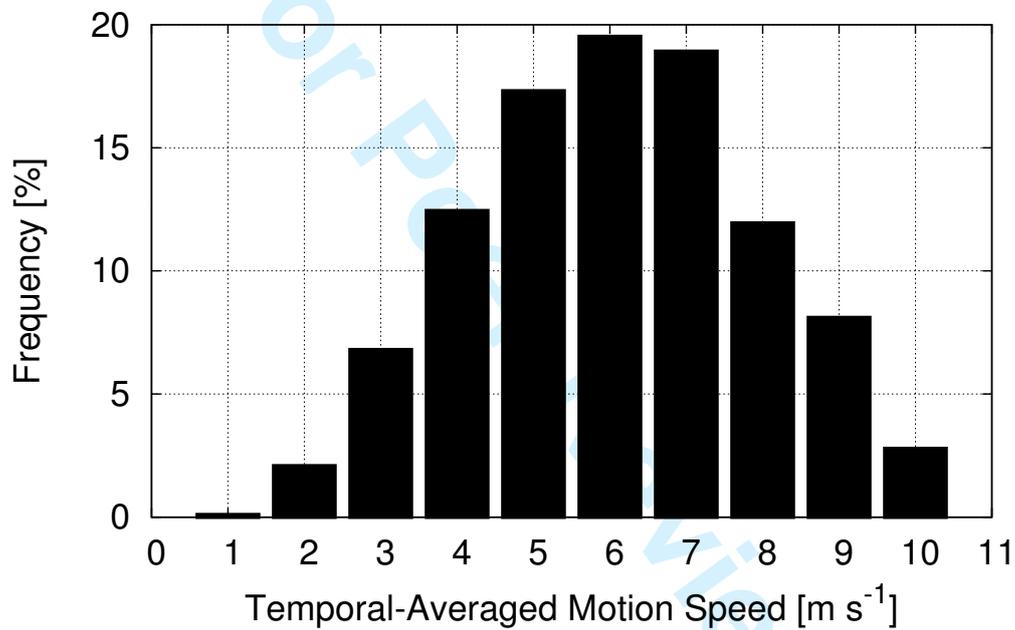
Figure 19. Frequency distribution of the time-averaged motion speed for the convective clusters, accumulated at the interval of 1 m s^{-1} and the range from v-0.5 to v+0.4, where v is a motion speed.

Q. J. R. Meteorol. Soc. **00**: 2–39 (2013)

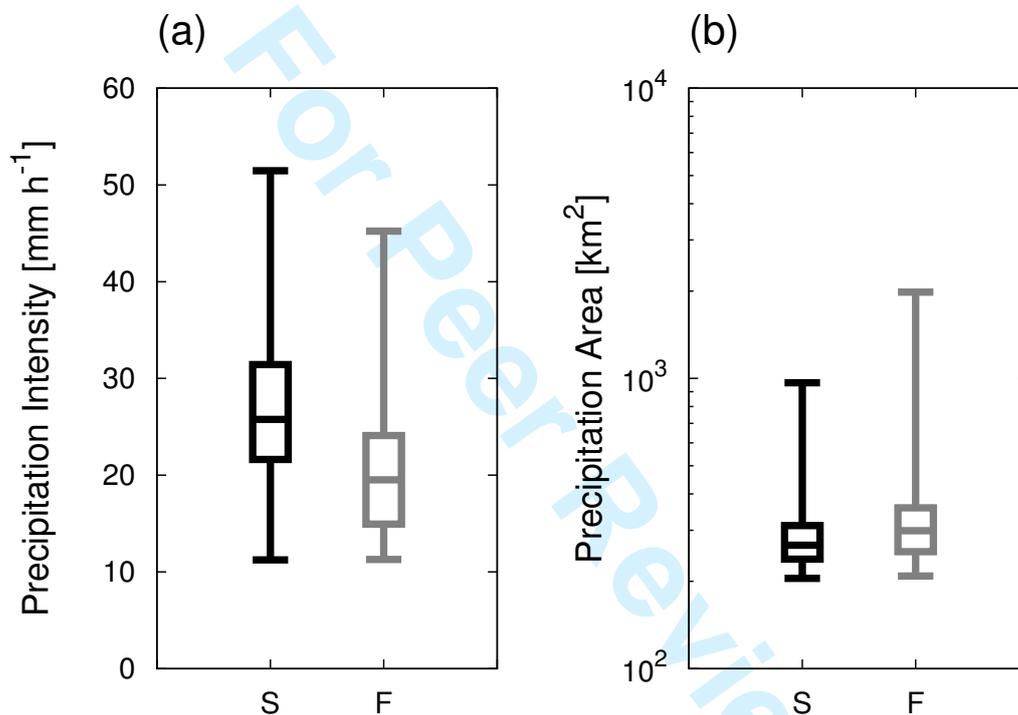*Prepared using qjrms4.cls*

Figure 20. The box-and-whisker plot of (a) precipitation intensity and (b) precipitation area for slow-moving (S) and fast-moving (F) categories. The whiskers at the upper and lower ends indicate the maximum and the minimum, respectively. The top and bottom lines of each box mean the 75 and 25 percentiles, respectively. The middle line in each box shows the median.
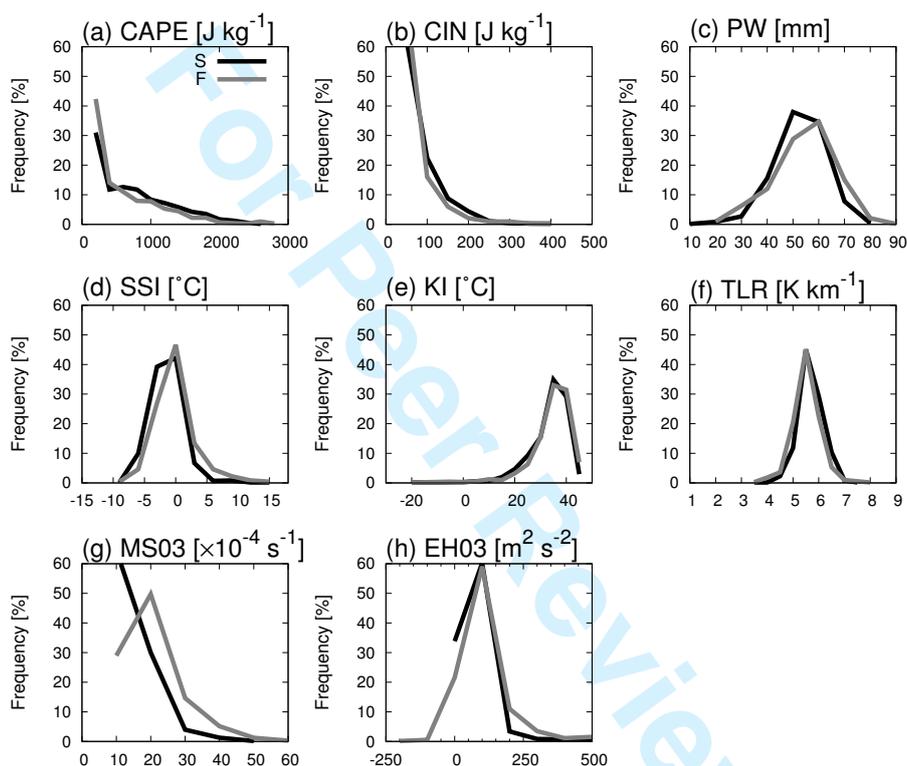
Figure 21. The same as Figure 13, except for slow-moving (S, black) and fast-moving (F, gray) categories. The frequency intervals in (a)–(h) are 200, 50, 10, 3, 5, 1, 5, and 50, respectively. The values show the frequencies that are accumulated at the center of the intervals.
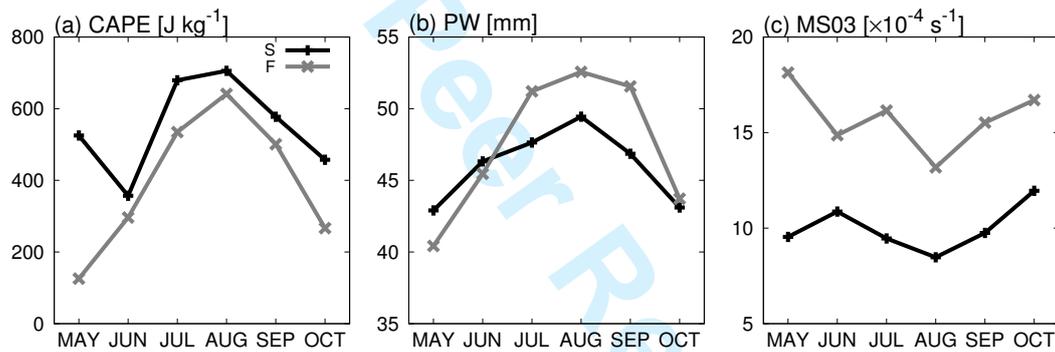
Copyright © 2013 Royal Meteorological Society

Q. J. R. Meteorol. Soc. **00**: 2–39 (2013)

Prepared using qjrms4.cls

Figure 22. Monthly values of the regional-mean values of (a) CAPE, (b) PW, and (c) MS03 for slow-moving (S, black) and fast-moving (F, gray) categories.

List of Tables

Table 1. The mean, standard deviation, and T-value of the environmental parameters between QSCCs (Q) and no-rain cases (N). Parameters with an asterisk ($*$) indicate that the mean values between Q and N are significantly different at the 95% confidence level.

Parameters	Average (Standard deviation)				T-value
	Q		N		(Q-N)
CAPE [J kg^{-1}]	489	(554)	69.7	(236)	35.8*
CIN [J kg^{-1}]	44.1	(58.5)	24.5	(63.2)	14.0*
PW [mm]	47.4	(11.5)	23.1	(11.8)	89.3*
SSI [C$^\circ$]	-1.9	(3.3)	1.4	(4.7)	-37.8*
KI [C$^\circ$]	30.7	(8.40)	7.98	(17.8)	85.1*
TLR [K km^{-1}]	5.31	(0.524)	5.29	(0.78)	1.28
MS03 [$\times 10^{-4}$ s^{-1}]	13.0	(7.83)	11.8	(6.23)	6.56*
EH03 [m^2 s^{-2}]	47.2	(107)	10.9	(61.7)	15.7*

Copyright © 2013 Royal Meteorological Society

Q. J. R. Meteorol. Soc. **00**: 2–39 (2013)

Prepared using qjrms4.cls

Table 2. The same as Table 1, except for slow-moving (S) and fast-moving (F).

Parameters	Average (Standard deviation)				T-value
	S		F		(S-F)
CAPE [J kg^{-1}]	625	(564)	486	(550)	4.71*
CIN [J kg^{-1}]	50.4	(56.8)	37.1	(53.5)	4.53*
PW [mm]	47.8	(9.35)	49.4	(11.5)	-2.93*
SSI [C$^\circ$]	-2.9	(2.6)	-1.6	(3.2)	-8.73*
KI [C$^\circ$]	30.9	(7.39)	31.8	(7.83)	-2.30*
TLR [K km^{-1}]	5.42	(0.444)	5.25	(0.507)	6.52*
MS03 [$\times 10^{-4}$ s^{-1}]	9.49	(5.73)	15.0	(8.26)	-14.5*
EH03 [m^{-2} s^{-2}]	22.1	(69.7)	61.9	(121)	-7.60*